Alternative Splicing of Latrophilin-3 Controls Synapse Formation

Shuai Wang[1,2,*], Chelsea DeLeon[3], Wenfei Sun[1,4], Stephen R. Quake[4,5], Bryan Roth[3], Thomas C. Südhof[1,2,*]

1. Department of Molecular and Cellular Physiology, Stanford University, Stanford, CA, 94305, USA

2. Howard Hughes Medical Institute, Stanford University, Stanford, CA, 94305, USA

3. Department of Pharmacology, UNC Chapel Hill School of Medicine, Chapel Hill, NC 27514, USA

4. Departments of Applied Physics and Bioengineering, Stanford University, Stanford, CA, 94305, USA

5. The Chan Zuckerberg Initiative, Redwood City, CA USA

*Co-corresponding authors (swang9@stanford.edu; tcs1@stanford.edu)

ABSTRACT

The assembly and specification of synapses in the brain is incompletely understood. Latrophilin-3, a postsynaptic adhesion-GPCR, mediates synapse formation in the hippocampus but the mechanisms involved remain unclear. Here we show that Latrophilin-3 organizes synapses by a novel dual-pathway mechanism: activation of $G_{\alpha S}$/cAMP-signaling and recruitment of phase-separated postsynaptic protein scaffolds. We found that cell type-specific alternative splicing of Latrophilin-3 controls its G protein coupling mode, resulting in Latrophilin-3 variants that predominantly signal via $G_{\alpha S}$/cAMP or via $G_{\alpha 12/13}$. CRISPR-mediated manipulation of Latrophilin-3 alternative splicing from a $G_{\alpha S}$- to a $G_{\alpha 12/13}$-coupled mode impaired synaptic connectivity to a degree similar to the overall deletion of Latrophilin-3, suggesting that $G_{\alpha S}$/cAMP-signaling by Latrophilin-3 splice variants mediates synapse formation. Moreover, $G_{\alpha S}$- but not $G_{\alpha 12/13}$-coupled splice variants of Latrophilin-3 recruit phase-transitioned postsynaptic protein scaffolds that are clustered by binding of presynaptic Latrophilin-3 ligands. Strikingly, neuronal activity promotes alternative splicing of the synaptogenic variant of Latrophilin-3. Together, these data suggest that activity-dependent alternative splicing of a key synaptic adhesion molecule controls synapse formation by parallel activation of two convergent pathways: $G_{\alpha S}$/cAMP signaling and the phase separation of postsynaptic protein scaffolds.

Synapse formation is central to the assembly of neural circuits in brain. This process is controlled, at least in part, by trans-synaptic complexes between adhesion molecules that function as signaling modules in organizing pre- and postsynaptic specializations[1,2,3]. Among various synaptic adhesion molecules, Latrophilin-3 (Lphn3; gene symbol *Adgrl3*) plays a prominent role in establishing Schaffer-collateral synapses formed by CA3-region axons on CA1-region pyramidal neurons in the hippocampus[4]. Lphn3 belongs to a family of postsynaptic adhesion-GPCRs (aGPCRs) that bind to the presynaptic adhesion molecules teneurin and FLRT[5,6,7]. Lphn3's function in synapse formation is known to require both its extracellular FLRT/teneurin-binding sequences and its intracellular regions, including its G protein-binding sequences[4,8], but the molecular mechanisms by which Lphn3 induces synapse formation remain elusive. In cell-signaling assays multiple G_{α} proteins were reported to couple to Lphn3[9,10,11,12] and their binding was confirmed by cryo-EM structures[13,14]. However, it is unknown which G_{α} protein physiologically mediates Lphn3-dependent synapse formation, it is unclear whether G_{α} protein signaling on its own constitutes the core mechanism of synapse formation, and it remains a puzzle how presynaptic ligand-binding to postsynaptic Lphn3 induces synapse formation.

Here, we show that Lphn3 gene (*Adgrl3*) transcripts undergo extensive alternative splicing. The resulting protein variants couple to different G_{α} proteins. Of these, the variant coupling to $G_{\alpha S}$ that induces cAMP production is the predominant splice variant expressed in brain and is essential for synapse formation in the hippocampus. Increasing neuronal activity switches the alternative splicing of Lphn3 towards the synapse-forming $G_{\alpha S}$-coupled variant. Strikingly, only the $G_{\alpha S}$-coupled Lphn3 splice variant recruits postsynaptic scaffold proteins. This recruitment occurs via the integration of the Lphn3 cytoplasmic tail onto the surface of phase-transitioned postsynaptic protein scaffolds. Finally, the presynaptic ligands Teneurin and FLRT synergistically promote clustering of Lphn3-containing postsynaptic scaffold protein condensates, explaining how trans-synaptic interaction could induce assembly of postsynaptic specializations. Both the synaptic function of Lphn3 and its ability to recruit phase-transitioned postsynaptic protein scaffolds require the C-terminal Lphn3 PDZ-binding motif (PBM) that interacts with Shank scaffold proteins. Our data outline a mechanistic pathway of synapse formation in which the various processes of $G_{\alpha S}$ signaling, phase separation, and trans-synaptic ligand binding mediate the assembly of postsynaptic

specializations. This pathway is controlled by the alternative splicing of Lphn3, enabling precise regulation of synapse formation by neuronal activity.

Extensive alternative splicing of Lphn3 (*Adgrl3*) transcripts

To comprehensively profile the alternative splicing pattern of Lphn3, we analyzed full-length mRNA transcripts from mouse retina and cortex[15]. We identified 5 principal sites of Lphn3 alternative splicing (Figure 1a; Extended Data Figure 1a). Among these, alternatively spliced Exons 6 and 9 encode extracellular sequences that are known to regulate binding to the presynaptic ligand Teneurin[7,16], while Exon15 encodes a 13 amino acid sequence within the extracellular GAIN domain. On the cytoplasmic side, Exon24 encodes a sequence in the 3rd intracellular loop of the 7-TMR GPCR region of Lphn3. The most extensive alternative splicing of Lphn3 is observed in the C-terminal sequence, which is encoded by Exons 28-32. Following the constitutively included Exon27, all Lphn3 transcripts contain either Exon31 or Exon32. Exons 28-30 are variably included in transcripts containing Exon31 but not in transcripts containing Exon32. Of these, Exons 28 and 29 are in-frame but Exon30 can be included in Lphn3 transcripts as Exon30a (using an internal splice-donor site) or Exon30b (passing the internal splice-donor site), of which Exon30b shifts the reading frame of Exon31 (Figure 1b, Extended Data Figure 1b). As a result, Lphn3 transcripts encode three distinct C-terminal sequences. The longest Lphn3 C-terminus is encoded by Exon31 without or with inclusion of Exons 28, 29, and 30a. The other two shorter C-terminal sequences are either encoded by Exon32 alone or by the Exon30b-31 sequence without or with inclusion of Exons 28 and 29 (Figure 1a). Transcriptome analyses of Lphn1 (*Adgrl1*) and Lphn2 (*Adgrl2*) revealed that of the Lphn3 sites of alternative splicing, the sites corresponding to Exons 9 of Lphn3 are conserved in Lphn1 and Lphn2, and that all latrophilins have multiple alternatively spliced 3' exons, but that the sites corresponding to Exons 15 and 24 of Lphn3 are conserved only in Lphn2 (Extended Data Figure 2a-d).

To assess the cell-type specificity and relative abundance of various Lphn3 transcripts, we analyzed deep RNAseq data obtained using ribosome-bound mRNAs that were isolated from different types of neurons[17]. We found that mRNAs containing Exon31 were more abundant (60-80% total) than mRNAs containing Exon32 (20-40%), with fewer mRNAs containing Exon30b (20-25%) (Figure 1c; Extended Data Figure 1c). Alternative splicing was

cell type-specific, such that inhibitory neurons harbored a higher prevalence of mRNAs containing Exon31 and 30b than excitatory neurons (Figure 1c; Extended Data Figure 1d, 1e), with different subtypes of neurons exhibiting diverse patterns of alternative splicing (Extended Data Figure 1c). Moreover, for some sites of alternative splicing developmental regulation was observed, such as for Exon30b that was preferentially included early postnatally but excluded during maturation of the brain (Extended Data Figure 3).

Lphn3 alternative splicing controls G-protein coupling

Given that the alternatively spliced Lphn3 sequences at the cytoplasmic sides are proximal to its G protein interaction site[13,14], we next systematically analyzed G protein coupling of the principal Lphn3 splice variants (Figure 1d, left) using the TRUPATH assay which affords an unbiased analysis of transducer coupling to GPCRs[18]. The alternative splicing pattern of Exons 24, 30b, 31, and 32 produces 6 principal splice variants that we analyzed. Dramatic differences emerged between Lphn3 splice variants in their G protein coupling preferences (Figure 1d, middle). The most abundant Lphn3 splice variant in the hippocampus (E24+/E30b-/E31+/E32-; Extended Data Figure 1, 3) preferentially couples to $G_{\alpha S}$ and less strongly to $G_{\alpha 12/13}$. If Exon31 is replaced by Exon32 (E24+/E30b-/E31-/E32+), Lphn3 predominantly couples to $G_{\alpha 12/13}$. Inclusion of Exon 30b, or exclusion of Exon 24 also shifts Lphn3 Gα coupling from $G_{\alpha S}$ to $G_{\alpha 12/13}$ (Figure 1d; Extended Data Figure 4). The role of Exon 24 in the 3rd cytoplasmic loop of Lphn3 is consistent with recent studies revealing the importance of this sequence in controlling G protein coupling[19], but the effect of the C-terminal alternative splicing of Lphn3 on G_{α}-protein coupling is surprising given that the sequences involved start 81 residues downstream of the last transmembrane region. These C-terminal sequences are not resolved in present cryo-EM structures of Lphn3 complexed to G proteins[13,14].

As an orthogonal approach to confirm the TRUPATH data, we measured the ability of various Lphn3 splice variants to increase cAMP levels in HEK293 cells. Upon co-expression of the cAMP reporter Pink Flamindo2[20] with Lphn3 splice variants in HEK293 cells we observed an increased cAMP level only when the Lphn3 splice variant that preferentially couples to $G_{\alpha S}$ was present (Figure 1d; Extended Data Figure 5a, 5b). The Lphn3-induced

signal was quenched by co-expressed PDE7b, a cAMP-phosphodiesterase, confirming its specificity. We conclude that alternative splicing of Lphn3 controls its G_α specificity, with the most abundantly expressed Lphn3 splice variants in the hippocampus preferentially coupling to $G_{\alpha S}$.

Lphn1 and Lphn2 have also been associated with different G_α proteins in previous studies [21,22,8], prompting us to study their G_α protein coupling modes. For Lphn1 and Lphn2 we again observed preferential coupling to $G_{\alpha S}$ for the tested splice variants (Extended Data Figure 2e). Viewed together, these data reveal that alternative splicing regulates G_α protein preference with $G_{\alpha S}$ being the predominantly coupled G_α protein for more abundant latrophilin transcripts, suggesting a possible explanation for the discrepancies among previous studies regarding the signaling pathways controlled by latrophilins.

CRISPR-mediated genetic manipulation of Lphn3 alternative splicing

To understand whether various Lphn3 splice variants are active in synapse formation under physiological conditions, we focused on its two most abundantly expressed C-terminal exons in the hippocampus: Exon31 and 32, which are coupled to different G_α protein signaling pathways and are alternatively spliced in a mutually exclusive pattern (Extended Data Figure 1a). To control the expression of these two exons from the endogenous Lphn3 gene, as opposed to using overexpressed Lphn3 splice variants in rescue experiments, we designed an acute CRISPR-Cas9 mediated genetic manipulation. In this approach, we selectively deleted the alternatively spliced Exon31 by targeting its splice-acceptor sequence with a guide-RNA, using a non-targeting guide-RNA as a control, and compared the loss of Exon31 to the loss of total Lphn3 proteins by targeting the constitutive N-terminal Exon7 (Figure 2a).

In primary hippocampal cultures, the acute CRISPR-mediated total Lphn3 deletion rendered Lphn3 protein undetectable by immunoblotting, whereas the Exon31-specific Lphn3 deletion or the control guide-RNA had no apparent effect on Lphn3 protein levels as quantified in multiple experiments (Figure 2b). Both quantitative RT-PCR and RNAseq analyses from neurons with a targeted deletion of only Exon31 uncovered a ~60% decrease in the level of Exon31-containing mRNAs and a ~100% increase in the level of Exon32-containing mRNAs

(Figure 2c, Extended Data Figure 5c). When Lphn3 protein was deleted by targeting Exon7, we observed a ~60% loss of mRNAs containing Exon31 or Exon32, with the decrease in mRNA levels being presumably due to non-sense mediated mRNA decay of the mutant mRNAs[23]. Transcriptomic analyses detected no off-target effect for either genetic manipulation, and no regulatory function for Lphn3 in gene expression (Figure 2d; Extended Data Figure 5d). These results validate the efficiency and specificity of the CRISPR manipulation approach, with Exon7 targeting causing a complete loss of Lphn3 protein whereas Exon31 targeting induces a switch from Exon31-containing to Exon32-containing mRNAs.

Lphn3 coupling to G_α protein is essential for synaptic connectivity

We employed three approaches to test whether exclusion of Exon31, and thus eliminating $G_{\alpha S}$ coupling, affects the function of Lphn3 in synapse formation. First, we measured the network activity of cultured hippocampal neurons using Ca^{2+}-imaging (Figure 2e-2h). Neurons exhibit regular spiking in culture owing to their spontaneous activity that can be quantified in individual neurons (Figure 2f). Averaging the signals of individual neurons in the same recording period produces a “synchronous firing” trace (Figure 2f, 2g) that reflects the strength of the synaptic network[24,25]. Quantifications of synchronous firing of cultured neurons showed that the global loss of Lphn3 cause a highly significant decrease (~40%) in firing rate without altering the signal amplitude (Figure 2g, 2h). Strikingly, the Exon31-specific deletion produced a similar decrease in neuronal firing rate as the global loss of Lphn3 proteins (Figure 2h).

Second, we asked whether the decrease in firing rate might result, at least in part, from a decrease in excitatory synapse numbers. We quantified the excitatory synapse density in cultured hippocampal neurons after CRISPR-mediated deletions of either all Lphn3 proteins (Exon7-targeted guide-RNA) or of Lphn3 transcripts containing Exon31 that couple to $G_{\alpha S}$. Puncta that were positive for both a presynaptic (vGluT1) and a postsynaptic marker (Homer1) were quantified on dendrites (Figure 3a, 3b). Both the complete loss of Lphn3 and the Exon31-specific deletion produced a significant decrease in synapse density (Figure 3b).

Third, we tested the function of Exon31 *in vivo*. We used monosynaptic retrograde tracing by pseudo-typed rabies virus to map the connectivity of genetically manipulated starter neurons in the hippocampal CA1 region (Figure 3c). Again, both the loss of all Lphn3 expression and the switching from Exon31 to Exon32 caused a large decrease (~60%) in synaptic inputs to CA1 pyramidal neurons from the ipsi- and the contralateral CA3 region (Figure 3d, 3f). Inputs from the entorhinal cortex were unchanged since Lphn3 mediates formation of CA3→CA1 Schaffer-collateral but not of entorhinal cortex→CA1 synapses (Figure 3e, 3f)[4].

Using three independent methods, these data thus demonstrate that the Exon31-containing Lphn3 isoform coupled to $G_{\alpha S}$ is essential for Lphn3-mediated synaptic connectivity.

Exon31- but not Exon32-containing Lphn3 recruits phase-separated post-synaptic protein scaffolds

Given the importance of the C-terminal sequence of Lphn3 encoded by Exon31 in synapse formation, we asked whether Exon31 performs additional functions other than regulating G_{α} protein coupling. We noticed that only the Exon31-containing transcripts encode the PDZ domain-binding motif (PBM) at the C-terminus that interacts with Shank proteins[26,27] and that is conserved in all latrophilins (Figure 1a; Extended Data Figure 2a, 2b). Thus we sought to test biochemically if full-length Lphn3 could form a complex with postsynaptic scaffold protein networks that are composed of GKAP, Homer, PSD95 and Shank, which are known to form phase-separated protein assemblies[28] (Figure 4a).

We purified recombinant full-length Homer3 and PSD95 proteins and truncated GKAP and Shank3 proteins and showed that they are highly soluble individually (Extended Data Figure 6). When mixed, however, the proteins formed a postsynaptic density complex (the “GHPS” complex) via phase separation[28] that was detected as a sedimented pellet by centrifugation (Figure 4b) and as droplet-like structures by imaging (Figure 4d). When we added purified recombinant full-length Lphn3 containing Exon31 or 32 to the GHPS complex, Lphn3 containing Exon31 robustly co-sedimented with the GHPS complex, whereas Lphn3 containing Exon32 did not (Figure 4b, 4c; Extended Data Figure 7a, 7b). Moreover, when we truncated the last 3 amino acids of the PBM from Lphn3 containing Exon31 (termed as

"ΔPBM"), a mutation that is known to disrupt shank binding[26], co-sedimentation of Lphn3 was also impaired (Figure 4b, 4c). Furthermore, Lphn3 containing Exon31 was fully assembled on the GHPS complex droplets, whereas Lphn3 containing Exon32 or the PBM-deleted Exon31 were not enriched on the post-synaptic scaffold condensates (Figure 4d, 4e; Extended Data Figure 7c, 7d). Interestingly, Exon31-containing Lphn3 was highly enriched in the periphery of the droplets, suggesting that detergent-solubilized Lphn3 formed a layer on top of the post-synaptic scaffold network (Figure 4d, 4e; Extended Data Figure 4c, 4d). Because both Shank3 and PSD95 contain PDZ domains which could interact with the PBM of Lphn3 containing Exon31 (Figure 4a) and post-synaptic scaffold phase separation critically depends on Shank3 but only weakly on PSD95 (Extended Data Figure 7h), we conclude that the alternative splicing of Lphn3 at the C-terminus determines its ability to recruit postsynaptic scaffold proteins and that such recruitment requires the interaction between the PBM in Exon31 of Lphn3 and the PDZ domain in Shank3 or/and PSD95.

Teneurins (Tenms)[5] and Flrts[6] are single transmembrane region-containing adhesion molecules which bind to the extracellular region of Lphn3. Their binding to Lphn3 is thought to mediate the trans-synaptic interaction between axon terminals and post-synaptic spines[4]. We asked how Tenm2 and Flrt3 might affect the morphology of the phase-separated postsynaptic scaffold protein complex containing Lphn3. When the purified extracellular region of Tenm2 was added to phase-separated complex, we observed a partial clustering of monomeric droplets into dimers and trimers (Figure 4f, 4g; Extended Data Figure 7f, 7g). The addition of Flrt3 clustered the droplets into higher-order oligomers, presumably partially due to the higher affinity of Flrt3 (K_d = ~15 nM)[6] than Tenm2 (K_d = ~500 nM)[29] for Lphn3. Tenm2 and Flrt3 can bind to Lphn3 simultaneously[29,30] and acted synergistically in promoting the clustering of phase-transitioned droplets (Figure 4f, 4g). The clustering effect was not observed in Exon32-containing Lphn3 or PBM-deleted Exon31-containing Lphn3. Because Tenm2 is an obligatory dimer via disulfide bonds between EGF repeat domains[31] and Flrt3 forms dimers via its leucine-rich repeat domain[32,33], we posit that the dimerization of ligands promoted the intermolecular interaction of Lphn3 in adjacent droplets, resulting in the formation of clustered Lphn3-coated postsynaptic scaffold protein condensates (Figure 4h). The formation of reconstituted Lphn3-bound scaffold protein condensates is robust at various scaffold protein concentrations (Figure 4; Extended Data Figure 7, and 8a-8c) and stoichiometries (Extended Data Figure 8d) and at physiological salt concentrations

(Extended Data Figure 8e). Interestingly, fluorescence recovery after photobleaching (FRAP) experiments show that Lphn3 is more dynamic than most scaffold proteins, suggesting that Lphn3-Exon31 forms a fluidic shell on the surface of the scaffold protein condensates. The coating by Lphn3-Exon31 of the condensates, regardless of Tenm2/Flrt3-induced clustering, does not perturb the dynamics of scaffold proteins (Extended Data Figure 8f-8l). Together, these data suggest Exon31-containing Lphn3 recruits postsynaptic scaffold protein complexes to the post-synaptic site. When encountering Tenm2/Flrt3 from the axon terminal, the Lphn3-coated post-synaptic scaffold protein complexes assemble into higher-order clusters.

The PBM of Lphn3-Exon31 is required for excitatory synapse formation

Due to the crucial function of the Lphn3-Exon31 PBM for Lphn3-dependent post-synaptic scaffold protein assembly, we ask whether the PBM is also important for synapse formation in culture neurons. To this end, we designed a gRNA targeting the PBM of Lphn3-Exon31 (Extended Data Figure 9a). Amplicon sequencing showed that acute CRISPR manipulations in cultured hippocampal neurons using this gRNA deleted the PBM in ~70% of Lphn3 mRNAs (Extended Data Figure 9b, 9c). The deletion of the PBM had no effect on the total Lphn3 protein, Lphn3-Exon31 mRNA levels, or Lphn3 alternative splicing (Extended Data Figure 9d, 9e). Functionally, the loss of PBM in Lphn3 caused a significant decrease in excitatory synapse density (Extended Data Figure 9f, 9g), suggesting that the PBM of Exon31 in Lphn3 is important for excitatory synapse formation.

Neuronal activity promotes the splicing of the synaptogenic Lphn3 variant

Given the observed cell type-specific expression of Lphn3 alternative splice variants and their distinct functions in synapse formation, we asked whether alternative splicing of Exon31 and Exon32 may be regulated by neuronal activity. To this end, we analyzed three recent RNAseq datasets in which neurons in culture or in vivo were examined as a function stimulation[34,35]. All treatments increased cFos expression, a marker gene for activated neurons (Figure 5a-5c, left). We observed a highly significant shift of Lphn3 alternative splicing from Exons32 to Exon31 in all three datasets, including the in vivo studies (Figure

5a-5c). In contrast, we found no activity-dependent changes in the inclusion of SS4 of *Nrxn1* mRNAs as expected[36], serving as a negative control for the experiment.

To further assess the activity-dependent alternative splicing of Lphn3 in a more native state, we analyzed a high-resolution single-cell RNAseq dataset from the medial prefrontal cortex (mPFC)[37]. We classified neurons based on the expression level of immediate early genes (IEGs, Figure 5d left) into "IEG-low", "IEG-medium" and "IEG-high" groups, with IEG expression used as a proxy of intrinsic neuronal activity. The "IEG-high" group exhibited significantly lower levels of Exon32 and higher level of Exon31 than the other groups (Figure 5d-5f). Although an elevated total Lphn3 expression was detected with some stimulations (Extended Data Figure 10e), the consistent response of neurons upon activation from all datasets is the switch of alternative splicing towards producing the variant that promotes synapse formation.

Summary

Here we show that Lphn3 transcripts are subject to extensive alternative splicing that controls the G-protein coupling specificity of Lphn3 and its ability to recruit postsynaptic scaffolds. We demonstrate that the Lphn3 splice variant which is coupled to $G_{\alpha S}$ and mediates cAMP signaling is required for synapse formation in vivo, and that this splice variant not only enables $G_{\alpha S}$ and cAMP activation but also selectively recruits postsynaptic scaffolding by enabling the incorporation of Lphn3 onto the surface of phase-transitioned postsynaptic density protein complexes. Furthermore, we found that the phase-transitioned postsynaptic scaffold recruited by Lphn3 are clustered into larger assemblies by the presynaptic teneurin and Flrt ligands of Lphn3. These findings outline a synapse formation mechanism orchestrated by Lphn3 that is mediated by two parallel pathways, localized $G_{\alpha S}$/cAMP signaling and phase transitioning of postsynaptic scaffolding proteins. In this manner, neurons leverage alternative splicing to enable precise control of synapse formation. Finally, increased neuronal activity results in an increased abundance of the more synaptogenic splice variant of Lphn3, suggesting that Lphn3 alternative splicing contributes to activity-dependent synapse formation.

Acknowledgements

We thank J.H. Trotter and Z. Sun for help on imaging; H. Wang, K. Liakath-Ali, X. Chen, and J. Dai for helpful discussions. This work was supported by grants from National Institute of Mental Health to T.C.S (5R01 MH126929-02) and a Stanford Maternal & Child Health Research Institute Postdoctoral Support grant to S.W. (1220319-117-JHACT), and R24DK116195, the NIMH Psychoactive Drug Screening Program and the Michael Hooker Distinguished Professorship to B.L.R., and Swiss National Science Foundation to W.S. (SNSF 211053). S.R.Q. is a Chan Zuckerberg Investigator.

Author Contributions

S.W. performed all experiments and analyzed all data, except the TRUPATH assay which was performed by C.D. and supervised by B.L.R. and the single cell RNAseq data from the mPFC region for neuronal activity analysis which was performed by W.S. and supervised by S.R.Q.. S.W. and T.C.S. conceptualized the project, designed the experiments, and wrote the manuscript with input from all authors. All authors contributed to data analyses.

Data Availability

All raw data supporting the findings of this study are deposited in the Stanford Data Repository (https://purl.stanford.edu/nj297xj2116), except for the high-throughput sequencing data generated from this study which was deposited at Gene Expression Omnibus repository with accession code GSE240791.

Code Availability Statement

The codes used for this study will be deposited in the Stanford Data Repository (https://purl.stanford.edu/nj297xj2116).

Conflict of Interest

The authors declare no conflict of interest

Methods

Mouse handling. C57BL/6 (JAX # 000664) mice were used for tissue RT-PCR experiment, and CAG-Cas9 mice (JAX #024858) were used for all other experiments. Mice were weaned at postnatal day 21 and housed in groups of maximum 5 on a 12 hr light/dark cycle with food and water *ad libidum*, in Stanford veterinary service center. All procedures conformed to National Institutes of Health Guidelines for the Care and Use of Laboratory Mice and were approved by the Stanford University Administrative Panel on Laboratory Animal Care.

Plasmids. Plasmids for the TRUPATH assay were from the Roth lab (Addgene #1000000163). Pink flamindo 2, GFP, and PDE7b constructs were from previous study[8]. Mouse Lphn3 of specified splicing variants (all have the following splicing configuration: -E6/+E9/+E15/-E28/-E29) were cloned into pCMV vector using In-Fusion® HD assembly. For manipulating Lphn3 KO, Lphn3 E31 KO, or Lphn3 E31 ΔPBM, gRNAs were cloned into lentiCRISPR v2 (Addgene #52961), followed by hsyn1 promoter driven EGFP (for calcium imaging and RNAseq), or mScarlet-I (for synapse puncta staining), or Cre recombinase (for monosynaptic rabies tracing), using In-Fusion® HD assembly. jRGECO 1a[38] was cloned into FSW lentiviral vector. GKAP, Homer3, PSD95, Shank3 coding regions[28] containing N-terminal 6xHis and 3C protease cleavage site were cloned into pCT10 vector. N-terminal flag tagged-Lphn3 E31 and Lphn3 E32 (with full splicing combination: E31: -E6/+E9/+E15/+E24/-E28/-E29/-E30/+E31, E32: -E6/+E9/+E15/+E24/-E28/-E29/-E30/+E32) were cloned into lenti_CMV-TetO2 vector. Sequences of all constructs were confirmed by Sanger sequencing at Elim Biopharm Inc, or long-read sequencing at Primordium.

Genetic CRISPR manipulations. 4 gRNAs were designed in this study. The control gRNA was designed to have no target in the mouse genome. The Lphn3 KO gRNA targets the constitutive exon 7 to induce frameshift. The Lphn3 E31 gRNA targets the splicing acceptor site immediate upstream of exon31, to disrupt the inclusion of Exon31. The Lphn3 E31 ΔPBM gRNA targets the PBM of Lphn3.Potential off-targets were assessed by Cas-OFFinder[39] to ensure specificity.

Generation of reference exon list. The exon coordinates of Lphn3 were extracted from GFF annotation of mouse genome GRCm38/mm10. Non-overlapping exons were named numerically in ascending order from 5' to 3' of the transcript. For exons with overlapping region (mostly due to alternative splicing donor/acceptor site), they were named with the same number but different alphabets. For exons at the 5' and 3' UTR only the longest annotated exons were used, since current study focuses on the coding region. This generated the draft of exon list. Because annotated exon list may contain exons which never translate to proteins (mostly due to incomplete splicing / incorrect annotation), the draft exon list was used to map the reads of Lphn3 from Ribotaq sequencing dataset[17] which is highly enriched for translating mRNAs, during which only exons detected in this dataset was preserved to produce the final reference exon list for this study.

Analysis of high-throughput sequencing data. This study analyzed six datasets from published studies and two datasets generated from this study:

(1) Reads from Pacbio long-read mRNA sequencing data[15] were aligned to reference genome (GRCm38/mm10) using gmaps. Reads belonging to Lphn3 from above 5 tissue samples (4

developmental stages of retina and P35 of cortex) were combined to increase the read depth, for analyzing the abundance of full-length transcripts.

(2) Cell type-specific Ribotaq sequencing data[17] reads were aligned to reference genome (GRCm38/mm10) using STAR. Reads belonging to Lphn3 were used for calculating percent spliced in (PSI) of exons.

(3) Neuronal activity regulated bulk transcriptome dataset (KCl and kainate treated)[34] and picrotoxin treated[35] were downloaded from GEO with accession number GSE175965, and GSE GSE104802. Reads were aligned as above using STAR. Reads belonging to Lphn3 were used for calculating percent spliced in (PSI) of exons.

(4) Native neuronal activity from mPFC region used single cell RNAseq dataset[37]. Smartseq reads were mapped to a custom genome, and individual Lphn3 exons were counted individually. Cells were unbiasedly clustered based on their transcriptomes. Immediate early genes were identified by ranking each genes' correlation to *Fos* expression. An IEG score was calculated by combining the expression of *Fos*, *Ier2*, *Egr1*, *Junb*, and *Dusp1*, which was used to categorize the activation status of each cell. Single neurons with at least one count for Exon31 or Exon32 were used for splicing analysis.

(5) Reads of Lphn3 KO and Lphn3 E31 KO studies of this work were aligned as above. HTseq was used to count reads. Only genes with more than 350 reads were used for DEseq2 analysis.

(6) Reads of PBM deletion from amplicon sequencing dataset were aligned as above. Paired-reads sequences near the edited site were extracted and the length of each read was calculated. Insertion/deletion which caused frameshift and mutation within the PBM region were classified as PBM KO events.

(7) Single cell RNAseq in primary visual cortex and anterior lateral motor cortex dataset from the Allen Institute[40] has processed read densities publicly available.

Calculation of exon percent spliced in (PSI). PSI is the percentage of reads containing target exon among all reads at target region. For alternative exon containing both 5' and 3' flanking exons (exon 24 and 30b for example), only the reads spanning the target exon-exon junctions were used for calculation. For alternative exons at the 3' termini (exon31 and exon32), all reads containing the target exon were used for calculation since the 3' termini of Lphn3 ends with either Exon31 or 32. Exon31 and 32 reads were normalized by exon length before calculating PSI.

Sample preparation of Lphn3 KO and Lphn3 E31 KO neurons for next-generation sequencing. Primary hippocampal culture neurons were infected with lentiviruses expressing gRNAs (control, Lphn3 KO, Lphn3 E31-only KO) at DIV3 and maintained till DIV14. One coverslip of culture was resuspended with 200 µl TRIzol® on ice, mixed with 50 µl chloroform, and incubated at RT for 2 min. Samples were centrifuged at 12000 g for 15 min at 4˚C in Eppendorf 5417C centrifuge. The aqueous layers were added to 100 µl ice-cold isopropanol for thorough mixing before incubation at -80˚C for 1 hr. Samples were thawed on ice and centrifuged at 20817 g for 20 min at 4˚C in Eppendorf 5417C centrifuge. Pellets were washed by 0.5 ml ice cold 75% EtOH before centrifuged at centrifuged at 20817 g for 10 min at 4˚C, and subsequently resuspended by 40 µl ddH2O containing 0.2 U/µl SUPERase•In™ RNase Inhibitor. Total RNA samples were converted to library using Illumina Stranded mRNA kit and sequenced in NovaSeq (PE 150) with 40M paired reads at Medgenome Inc.

Sample preparation of ΔPBM neurons for amplicon sequencing. Primary hippocampal culture neurons were infected with lentiviruses expressing gRNAs (control or ΔPBM) at DIV3 and maintained till DIV14. Total RNA samples were extracted as above, converted to cDNA using PrimeScript™ RT-

PCR Kit. PBM region of Lphn3 was amplified using primer: 5'-AAACCTGGGCTCCAGAAACC-3', 5-GGAAAGATTGGGGCACAGGA-3', and converted to library using Nextera XT adaptor/indexes, and sequenced in MiSeq at Stanford Functional Genomics Facility.

TRUPATH G-protein coupling assay. HEK293T cells were obtained from ATCC and maintained, passaged and transfected in DMEM medium containing 10% FBS, 100 U ml^{-1} penicillin and 100 µg ml^{-1} streptomycin (Gibco-ThermoFisher) in a humidified atmosphere at 37 °C and 5% CO_2. After transfection, cells were plated in DMEM containing 1% dialyzed FBS, 100 U/mL penicillin, and 100 µg/mL streptomycin for BRET assays. Constitutive activity of Lphns were accomplished using the previously optimized Gα-Rluc8, β-subunit, and N-terminally tagged γ-GFP2 subunit pairs described before[18]. HEK cells were plated in a 12-well plate at a density of 0.3-0.4x10^6 cells per well with DMEM containing 10% FBS, 100 U/mL penicillin, and 100 µg/mL streptomycin. Six hours later, cells were transfected with a 1:1:1 ratio of optimized Gα:β:γ pairings at 100 ng and various amounts of receptor (25 ng, 50 ng, 100ng, 200 ng, 300 ng) using TransIt-2020 (Mirius Bio). To establish a baseline for the cells, pcDNA was used at 100 ng and referred to as 0 ng. The following day, cells were removed from the 12-well plate with trypsin and seeded in a 96-well white, clear-bottomed plate (Greiner Bio-One) with DMEM containing 1% dialyzed FBS at a cell density of 30,000-35,000 cells per well. Cells were incubated overnight to allow for attachment and growth. The next day, media was aspirated from the wells. A solution of assay buffer (20 mM HEPES, Hank's balanced salt solution, pH 7.4) and 5 µM of coelentrazine 400a (Nanolight Technology) was prepared and added to each well. Cells were allowed to equilibrate with the coelentrazine 400a in the dark for 10 minutes. Corresponding BRET data was collected using a Pherastar FSX Microplate Reading with luminescence emission filers of 395 nm (RLuc8-coelentrzine 400a) and 510nm (GFP2) and an integration time of 1 sec per well. BRET ratios were calculated as a ratio of the GFP2:RLuc8 emission. The constitutive coupling (0 ng) was used as the baseline to subtract NET BRET of the experimental conditions for each receptor. 3 independent cultures with 7 technical replicates in each culture were used in total.

cAMP reporter assay. HEK293T cells were maintained in DMEM+10% FBS at 37˚C 5% CO2, and seeded onto 24-well plate. During calcium transfection of each well, EGFP (0.23 µg), pink flamindo2 (0.2 3µg), GαS (0.16 µg), Gβ (0.16 µg), Gγ (0.16 µg) were used for all conditions. When indicated, additional constructs were co-transfected including PDE7b (0.23 µg) and 6 isoforms of Lphn3 (E24+/E30b-/E31+/E32-, E24+/E30b+/E31+/E32-, E24+/E30b-/E31-/E32+, E24-/E30b-/E31+/E32-, E24-/E30b+/E31+/E32-, E24-/E30b-/E31-/E32+, 0.23 µg each). 16 hr post-transfection, medium was replaced by 0.5 ml DMEM+10% FBS. 36-48 hr post transfection, medium of all cultures were replaced by 0.5 ml imaging buffer (20mM Na-Hepes pH7.4, 1x HBSS (gibco #14065056)) and incubated at RT for 30 min. When indicated, 2.5 µM Forskolin and 5 µM IBMX added to the culture for 5 min. Imaging was performed under Nikon confocal microscopy at 10x objective.

Primary hippocampal neuron culture. Neonatal P0 mice pups of CAG-cas9 mice (JAX #024858) were dissected in ice cold HBS to obtain hippocampi, which were digested in 1% v/v papain suspension (Worthington) and 0.1 U/µl DNaseI (Worthington) DNaseI for 15min at 37˚C. Hippocampi from 2 pups were washing with calcium-free 1xHBS (pH7.3) and dissociated using gentle pipetting in plating medium (MEM containing 5% FBS, 0.6% glucose, 2% Gem21 NeuroPlex™ Supplement, 2 mM GlutaMAX™), filtered through 70 µm cell strainer, and seeded onto Corning® Matrigel®-coated 12 mm cover glasses in one 24-well plate, and maintained at 37˚C 5% CO2. 16 hr post seeding (DIV1), 90% media were replaced by maintenance medium (Neurobasal A with 2% Gem21

NeuroPlex™ Supplement, 2 mM GlutaMAX™). At DIV 3, 50% of medium were replaced with fresh maintenance medium supplemented 4 μM Ara-C (Cytosine β-D-arabinofuranoside hydrochloride), and lentivirus expressing gRNA. When indicated, lentiviruses expressing jRGECO1a were added at DIV7. At DIV7, 10, and 13, 30% media were replaced with fresh maintenance medium, before analyzing at DIV14.

Virus preparation. Lentiviruses were produced in HEK293T cells using the 2nd generation packaging system. Per 150 cm^2 of cells, 186 μl 2 M $CaCl_2$ containing 5.8 μg of lentivirus shuttle vector, 2.5 μg pVSVG (addgene 12259), 4.2 μg Gag-Pol-Rev-Tat (addgene 12260) at a total volume of 1.5 ml was added dropwise to an equal volume of 2X-HBS (280 mM NaCl, 10 mM KCl, 1.5 mM Na_2HPO_4, 12 mM glucose, and 50 mM HEPES, pH 7.11) under constant mixing, incubated for 15 min at room temperature, and added dropwise to the cells. 8-12hr post-transfection, medium was replaced by DMEM with 10% FBS. 48 hr post-transfection, cell medium was cleared by spinning at table-top centrifuge at 2000 g for 3 min, and filtered via 0.45 μm PES membrane. The viral supernatant was loaded onto 2 ml 30% sucrose cushion in PBS and centrifuged in Thermo Scientific SureSpin 630 rotor at 19000 rpm for 2 hr. Viral pellet was resuspended in 30 μl MEM and flash frozen in liquid nitrogen. AAVs (CAG-DIO-RG and CAG-DIO-TCB-mCherry) in capsid 2.5 and pseudotyped rabies virus RbV-CVS-N2c-deltaG-GFP (EnvA)[41] were prepared at Janelia Farm Viral core facility.

Monosynaptic retrograde rabies tracing. P0 neonatal mouse pups were anesthetized on ice for 4 min and head-fixed on by ear bars and 3D-printed mold. 0.35 μl 1x 10^9 IU/ml lentiviruses (hsyn1-gRNA-NLS-cre) were injected unilaterally to CA1 at coordinates AP +0.95 mm, ML -0.92 mm, DV -1.30 mm (zeroed at Lambda). At P21, mice were anesthetized by avertin (250 mg/kg) and head-fixed on stereotaxic injection rig, 0.2 μl AAVs CAG-DIO-RG 3.6 x 10^{12} GC/ml and CAG-DIO-TCB-mCherry 6.35 x 10^{12} GC/ml (1:1 volume mix) were co-injected to CA1 at coordinates AP -1.80 mm, ML -1.35 mm, DV -1.30 mm (zeroed at Bregma). At P35, the same CA1 site was injected by 0.15 μl EnvA-pseudo-typed rabies virus RbV-CVS-N2c-deltaG-GFP at 2 x 10^8 IU/ml. After the surgery, the incisions of P21 and P35 mice were closed by suture and 3M Vetbond tissue adhesive (# 1469SB). After all injections, mice were recovered on a heating pad before returning to home cage. At P42, mouse brains which had been perfused were fixed in 4% PFA (Electron Microscopy Sciences, EM grade #15714) in PBS for 4hr at RT, subsequently incubated in 30% w/v sucrose in PBS at 4˚C overnight, and cryopreserved in Tissue-Tek® O.C.T. compound (Sakura) on dry ice. Frozen tissue blocks were cut into 20 μm coronal sections on a cryostat and collected on glass slides (Globe Scientific #1358W). Sections were air-dried, stained in 1 μg/ml DAPI for 10 min, washed once with PBS, and sealed in Fluoromount-G® (Southern Biotech, 0100-01). Sections were imaged on Olympus VS200 slide scanner at 10x. 5-6 mice were used per condition for the study.

RT-PCR of Lphn3 alternative exons in tissues. C57BL/6 Mice at postnatal day (P4, P9, P14, P21, and P35) were euthanized and brains were dissected to isolate olfactory bulb, cerebellum, hippocampus, prefrontal cortex, striatum and retina. Tissues were grinded with 500 μl TRIzol® on ice, mixed with 125 μl chloroform, and incubated at RT for 2 min. Samples were centrifuged at 12000 g for 15 min at 4˚C in Eppendorf 5417C centrifuge. The aqueous layers were added to 250 μl ice-cold isopropanol for thorough mixing before incubation on ice for 5 min. Samples centrifuged at 20817 g for 20 min at 4˚C in Eppendorf 5417C centrifuge. Pellets were washed by 0.5 ml ice cold 75% EtOH before centrifuged at centrifuged at 20817 g for 10 min at 4˚C, and subsequently resuspended by 40 μl ddH2O containing 0.2 U/μl SUPERase•In™ RNase Inhibitor. 100 ng of total RNA was used for cDNA conversion by PrimeScript™ RT-PCR Kit using random 6mer. 1 μl cDNA

was used for PCR targeting exon-exon junction regions using Ex Taq™ DNA Polymerase. The following primers were used: β-actin (5'-TCTACAATGAGCTGCGTGT-3', 5'-CGAAGTCTAGAGCAACATAG-3'), Lphn3 E6 (5'-CCACAGCTACTCATCCTCAC-3', 5'-GCTCTCGATCATGATGACGT-3'), Lphn3 E15 (5'-GGGGACATCACCTACTCTGT-3', 5'-TCAGGTCTCTCCAGGCATTC-3'), Lphn3 E24 (5'-CCTGAATCAGGCTGTCTTGA-3', 5'-AAATGGTGAAGAGATACGCC-3'), Lphn3 E31 (5'-TCCAGGACGGTACTCCACA-3', 5'-GGCATTGTTCAGAAGCCCCT-3'), Lphn3 E32 (5'-TCCAGGACGGTACTCCACA-3', 5'-TCCTGTGTCCTGTTTCGGGA-3'). PCR program is: 94˚ 1min, 94˚C 30s, 55˚C 30s, 72˚C 1min, go to step2 for 30 times. PCR products were separation on 2% agarose gel in 1xTAE buffer and imaged using Biorad Gel imaging system.

RT-qPCR of Lphn3 KO and Lphn3 E31 KO neurons. 80ng total RNA for each culture was used for converting to cDNA by PrimeScript™ RT-PCR Kit using random 6mer. 1μl cDNA was used for qPCR experiment in TaqMan™ Fast Virus 1-Step Master Mix using PrimeTime Std® qPCR designed primer-probe sets (For β-actin: 5'-GACTCATCGTACTCCTGCTTG-3', 5'-GATTACTGCTCTGGCTCCTAG-3', /56-FAM/CTGGCCTCA/ZEN/CTGTCCACCTTCC/3IABkFQ/; for Lphn3 E27-E31 junction: 5'-CCTTCATCACCGGAGACATAAA-3', 5'-GTGGTAGAGTATCCATGACACTTG-3', /56-FAM/CA GCTCAGC/Zen/ATCGCTCAACAGAGA/3IABkFQ/; for Lphn3 E27-E32 junction: 5'-CAGTCAGAGTCGTCCTTCATC-3', 5'-GTCAGTCTCAGGTCCATAAGTC-3', /56-FAM/AACAGCTCA/Zen/GCATCGCTCAACAGA/3IABkFQ/). PCR program is: 95˚ 20s, 95˚C 3s, 60˚C 30s, go to step2 for 40 times. Ct values for Lphn3 E31 and E32 sample were subtracted by that of β-actin from the same sample to get ΔCt. All ΔCt values were normalized by control gRNA. 8 cultures were used in total.

RT-PCR of Lphn3 KO, Lphn3 E31 KO and ΔPBM in neurons. 80ng total RNA for each culture was used for converting to cDNA by PrimeScript™ RT-PCR Kit using random 6mer. 1μl cDNA was used 1 μl cDNA was used for PCR targeting exon-exon junction regions using Ex Taq™ DNA Polymerase. The following primers were used: β-actin (5'-TCTACAATGAGCTGCGTGT-3', 5'-CGAAGTCTAGAGCAACATAG-3'), Lphn3 E31 (5'-GTCAGAGTCGTCCTTCATCAC-3', 5'-AGTTGTTCACCAGTTTGTTCATC-3'), Lphn3 E32 (5'-CGGATTCGGAGAATGTGGAA-3', 5'-CCACAGATAACGTGTGTGGT-3'). The expression level of Exon31 and Exon32 were normalized by β-actin.

Immunoblotting analyses. One well of neuron culture from 24 well plate was lysed in 50μl lysis buffer (20mM Tris pH7.5, 500mM NaCl, 1% Tritonx100, 0.1% SDS 1xRoche EDTA-free protease inhibitor) at RT for 5min. 20μl 5x SDS loading buffer was added and the samples were subject to SDS-PAGE electrophoresis. Gels were transferred to 0.2μm nitrocellulose membrane in Trans-Blot Turbo Transfer system (Biorad) and blocked by western blocking buffer (5% BSA in 1xTBST) at RT for 30min. Mouse anti-Lphn3 (Santa Cruz Biotech #sc-393576, 1:1000) and mouse anti-actin (Sigma #A1978, 1:3000) antibodies in western blocking buffer were added and incubated at 4˚C for overnight. The membranes were washed in western blocking buffer three times for 10min each, and IRDye® 800CW Donkey anti-Mouse IgG Secondary Antibody (Li-cor # 926-32212, 1:20000) in western blocking buffer was added to the membrane which was incubate at RT for 1hr and washed in 1xTBST three times for 10 min each. Samples were imaged at Odyssey Imager (Li-Cor). Quantifications of Lphn3 level were normalized to β-actin.

Calcium imaging. Primary culture neurons were maintained as mentioned above, except they were infected with lentivirus expressing hsyn1-gRNA-EGFP at DIV3, and lentivirus expressing hsyn1-jRGECO1a at DIV7. At DIV14, the coverslips containing neuron were washed once with 37˚C warmed Tyrode buffer (25mM Na-HEPES pH7.4, 129mM NaCl, 5mM KCl, 2mM $CaCl_2$, 1mM $MgCl_2$, 15mM glucose and transferred to 12 well glass plate (Cellvis # P12-1.5H-N) in Tyrode buffer. After 30 min of incubation in Tyrode buffer at 37˚C 5% CO2, the cultures were imaged in Leica microscopy at 37˚C 5% CO2, with 50 ms exposure, 85 ms interval for 1 min for each field of view (FOV). 6-8 FOVs were recorded for each coverglass of culture. For each condition from one batch of culture, 3-5 cover glasses of cultures were imaged. 3 batches of culture were used in total.

Immunohistochemistry and synapse puncta imaging. Primary hippocampal neurons were washed in Tyrode buffer (25 mM Na-HEPES pH 7.4, 129 mM NaCl, 5 mM KCl, 2 mM $CaCl_2$, 1 mM $MgCl_2$, 15 mM glucose) and fixed in 4% PFA, 4% sucrose in 1 x DPBS at 37˚C for 15 min. Afterwards, neurons were washed three times with 1xDPBS for 5 min each, and permeabilized in 0.1% Triton X-100 in 1x DPBS for 10min at RT without shaking. After blocking with 0.5% fish skin gelatin in 1x DPBS at 37˚C for 1hr, culture was stained with chicken anti-MAP2 (Encor #CPCA-MAP2, 1:1000), guinea pig anti-vGluT1 (Milipore #AB5905, 1:1000), and rabbit anti-Homer (Milipore #ABN37, 1:1000) in blocking buffer at 4˚C for overnight. Samples were washed three time with 1xDPBS for 8 min each, and incubated with secondary antibodies (anti-chicken Alexa405, anti-guinea pig Alexa647, and anti-rabbit Alexa488) in blocking buffer at 37˚C for 1hr. Afterwards, the culture coverslips were washed three times with 1x DPBS for 8 min each, once with ddH2O briefly, before loaded onto glass slide slides (Globe Scientific #1358W) in Fluoromount-G® (Southern Biotech, 0100-01) and sealed in nail polish (Amazon #B000WQ9VNO). Samples were imaged under Nikon confocal microscopy at 60x, with 0.35 µm step size and 4-6 z-stacks. For each coverglass of culture, 20-25 neurons containing well-isolated dendrites were imaged. For each condition of one batch of culture, 2 cover glasses of culture were imaged. 3 batches of culture were used in total.

Image analyses. Five types of image analyses were performed.

1. **Quantification of excitatory synapse puncta density.** Maximum intensity files were produced from z-stacked images. Background was subtracted and the 5-10 well-isolated secondary dendrites were cropped from each neuron in Fiji (v 2.9.0) for processing. Excitatory synapses, especially in mature mushroom spines, are localized ~0.5-1µm away from the dendrite due to the long neck of the spine[3]. Our confocal images have interpixel unit of 0.20714 µm/pixel. Thus, in our analyses we include vGluT1/Homer signals within 5 pixels away from dendrite. The cropped files were converted to binary images using the same threshold for the same channel, for the same batch of experiment. For calculating excitatory synapse puncta, the vGluT1 and Homer binary images were used to product overlapped region.Binary regions containing more than 2 neighboring pixels was considered as puncta, which were searched and quantified using scikit-image (v 0.20.0) package[42]. To calculate dendrite length, binary MAP2 channel images were skeletonized by scikit-image to 1 pixel representation whose length was measured by FilFinder (v 1.7.3) package[43]. For each cropped file, the puncta number divided by dendrite length produced the puncta density. All imaged regions from one batch of experiment were averaged to calculate the puncta density for one condition. 3 batches of data were plotted in total.

2. **Calcium imaging.** Time-lapsed videos of calcium imaging files were processed by CaImAn package[44] to search for spiking somas and generate corresponding fluorescence intensity (ΔF/F) over time. The key parameters were: decay_time =0.4, p=1, gnb=2, merge_thr=0.85, rf=60,

stride_cnmf=6, K=10, gSig=[40,40], method_init='greedy_roi', ssub=1, tsub=1, min_SNR=200, rval_thr=0.85, cnn_thr=0.99, cnn_lowest=0.1. ΔF/F traces of all detected spiking somas from one field of view were averaged to produce one synchronized firing trace. SciPy (v1.10.1)[45] algorithm "find_peaks" (height=0.15, width=(2,20), distance=20) was used to detect the spiking number and signal strength (ΔF/F) for each synchronized firing trace. The synchronizing firing rate was calculated by dividing spiking number against total time for each trace. To plot the firing rate (or ΔF/F) for each condition, the median of firing rate (or ΔF/F) from all traces of one batch was used. 3 batches of culture were plotted in total.

3. **Rabies tracing.** Coronal sections corresponding to Bregma -1.55 to -2.03 mm[46] for hippocampal formation and Bregma -3.8 to -4.1 mm[46] for lateral entorhinal cortex (LEC) were processed in Fiji by background subtraction. Regions of ipsilateral CA1, ipsilateral CA3, contralateral CA3, and ipisilateral LEC were cropped in Fiji for processing in scikit-image (v 0.20.0). Cropped regions were converted to binary images using the same threshold for the same channel, for the same batch of experiment. Binary regions containing more than 80 neighboring pixels (red channel for CA1) and 150 neighboring pixels (green channel for CA3 and LEC) were considered as neuron soma, and were counted by scikit-image[42] functions "measure.label" and "measure.regionprops". All counts from one mouse were used to calculate connectivity strength of ipsilateral CA3-CA1, contralateral CA3-CA1, LEC-CA1.

4. **cAMP imaging using Pink Flamindo 2**. After background subtraction, 488 and 546 channel signal from one field of view was used to calculate pink flamindo 2/GFP. 3-10 fields of view were imaged per condition per batch of culture. 3 batches of cultures were used in total.

5. **Phase-transitioned droplet.** After background subtraction, signals from indicated channels were used for analysis. 12.86μm linear region across the diameter of the droplets were used to plot the signal from the edge to the center of the droplets. To calculate the number of droplets per cluster, contacting droplet were counted as one cluster. scikit-image (v 0.20.0) package[42] was used to count the size of droplets. 3 independent replicates were used for each experiment.

Protein purification. We used truncated GKAP and Shank3 to retain essential interaction modules and obtain soluble proteins. 6xHis-tagged GKAP, Shank3, Homer3 and PSD95 were purified as before[28] with slight modifications. Constructs were transformed to BL21 (DE3) pLysS, which were induced at OD_{600}=0.6 with 0.25mM IPTG at 16˚C for 18hr. Cells were lysed in Ni-buffer A (20 mM Tris pH8, 500 mM NaCl, 5% glycerol, 4 mM BME, 20 mM Imidazole, 1x roche EDTA-free protease inhibitor, 100 U/ml benzonase) and cleared at SS34 rotor at 14000 rpm for 30 min at 4˚C. Proteins were loaded onto Ni-NTA column, washed in Ni-buffer A and eluted in Ni-buffer B (20 mM Tris pH8, 250 mM NaCl, 5% glycerol, 4 mM BME, 400 mM Imidazole). His-tags were removed by 3C protease. Finally, the proteins were purified in size exclusion column (SD75 10/300 for GKAP, and SD200 10/300 for others) in SEC buffer (20 mM Tris pH8, 300 mM NaCl, 2 mM DTT). Lentiviruses containing CMV-TetO_2-Flag-Lphn3 E31, E32 and E31 ΔPBM were used to express proteins in FreeStyle™ 293-F Cells at 37˚C 8% CO_2, and purified based on previous method[13]. 6xHis-tagged TEN2 and FLRT3 were cloned into pCMV vector and expressed in Expi293F™ cells. 4 days post-transfection, medium was harvested and loaded onto Ni-NTA column, washed in Ni-buffer C (20 mM Hepes pH7.4, 150 mM NaCl, 20 mM Imidazole pH7.6) and eluted in Ni-buffer D (20 mM Hepes pH7.4, 150 mM NaCl, 250 mM Imidazole pH7.6). His-tags were removed by 3C protease, and the proteins were purified in size exclusion column (SD200 10/300) in SEC buffer (20 mM Hepes pH7.4, 150 mM NaCl).

Fluorescence labeling of proteins. NHS-dyes (AAT iFluor NHS-405, AAT iFluor NHS-488, AAT iFluor NHS-546, Invitrogen Alexa NHS-647) were added to the purified protein at 1:1 molar ratio, and the labeling proceed at RT for 1hr. Reaction was quenched by 100 mM Tris pH8.2. Free dyes were removed by desalting column.

Phase transition imaging and sedimentation assay. Protein mixtures were incubated at RT for 10-20 min. For imaging experiment, 5µl of sample was loaded onto channeled slide and imaged under confocal microscope. For pelleting experiment, supernatant was immediately removed and pellet was resuspended in 2 x SDS loading buffer. All samples were subject to SDS-PAGE electrophoresis and stained in Coomassie G-250 blue.

Fluorescence Recovery After Photobleaching experiment. After phase separation is completed, strong excitation laser intensities were used to bleach all channels of a small area for 10 seconds, after which the fluorescence were recorded for 6 min. Recovery traces were fitted into exponential equation $y = ae^{-bx} + c$ to extrapolate the $t_{1/2} = \frac{ln2}{b}$.

Statistical information. Most statistical tests used two-sided Student's t-test, as indicated. Differential gene expression of RNAseq data used DESeq2. Gene expression of single cell dataset used Wilcoxon-rank Sum Test (*p < 0.05; **p < 0.01; ***p < 0.001). Non-significant results (p>0.05) are not displayed. When applicable, boxplots (center line, median; box limits, first and third quartiles; minimal and maximum, minimal and maximum datapoint) show the distribution of datapoints (each point represents one datapoint). Error bar represents SEM or SD as indicated.

REFERENCES

1. Moreland, T. & Poulain, F. E. To Stick or Not to Stick: The Multiple Roles of Cell Adhesion Molecules in Neural Circuit Assembly. *Frontiers in Neuroscience* (2022) doi:10.3389/fnins.2022.889155.

2. Sanes, J. R. & Zipursky, S. L. Synaptic Specificity, Recognition Molecules, and Assembly of Neural Circuits. *Cell* **181**, 536–556 (2020).

3. Südhof, T. C. The cell biology of synapse formation. *J. Cell Biol.* **220**, 1–18 (2021).

4. Sando, R., Jiang, X. & Südhof, T. C. Latrophilin GPCRs direct synapse specificity by coincident binding of FLRTs and teneurins. *Science (80-.).* **363**, (2019).

5. Silva, J. P. *et al.* Latrophilin 1 and its endogenous ligand Lasso/teneurin-2 form a high-affinity transsynaptic receptor pair with signaling capabilities. *Proc. Natl. Acad. Sci. U. S. A.* **108**, 12113–12118 (2011).

6. O'Sullivan, M. L. *et al.* FLRT Proteins Are Endogenous Latrophilin Ligands and Regulate Excitatory Synapse Development. *Neuron* **73**, 903–910 (2012).

7. Boucard, A. A., Maxeiner, S. & Südhof, T. C. Latrophilins function as heterophilic cell-adhesion molecules by binding to teneurins: Regulation by alternative splicing. *J. Biol. Chem.* **289**, 387–402 (2014).

8. Sando, R. & Südhof, T. C. Latrophilin gpcr signaling mediates synapse formation. *Elife* **10**, 1–22 (2021).

9. Mathiasen, S. *et al.* G12/13 is activated by acute tethered agonist exposure in the adhesion GPCR ADGRL3. *Nat. Chem. Biol.* **16**, 1343–1350 (2020).

10. Kordon, S. P. *et al.* Isoform- and ligand-specific modulation of the adhesion GPCR ADGRL3/Latrophilin3 by a synthetic binder. *Nat. Commun.* **14**, (2023).

11. Moreno-Salinas, A. L. *et al.* Convergent selective signaling impairment exposes the pathogenicity of latrophilin-3 missense variants linked to inheritable ADHD susceptibility. *Mol. Psychiatry* (2022) doi:10.1038/s41380-022-01537-3.

12. Bui, D. L. H. *et al.* The adhesion GPCRs CELSR1–3 and LPHN3 engage G proteins via distinct activation mechanisms. *Cell Rep.* **42**, (2023).

13. Barros-Álvarez, X. *et al.* The tethered peptide activation mechanism of adhesion GPCRs. *Nature* **604**, 757–762 (2022).

14. Qian, Y. *et al.* Structural insights into adhesion GPCR ADGRL3 activation and Gq, Gs, Gi, and G12 coupling. *Mol. Cell* (2022) doi:10.1016/j.molcel.2022.10.009.

15. Ray, T. A. *et al.* Comprehensive identification of mRNA isoforms reveals the diversity of neural cell-surface molecules with roles in retinal development and disease. *Nat. Commun.* **11**, 1–20 (2020).

16. Wang, Y. *et al.* Adhesion GPCR Latrophilin 3 regulates synaptic function of cone photoreceptors in a transsynaptic manner. *Proc. Natl. Acad. Sci. U. S. A.* **118**, (2021).

17. Furlanis, E., Traunmüller, L., Fucile, G. & Scheiffele, P. Landscape of ribosome-engaged transcript isoforms reveals extensive neuronal-cell-class-specific alternative splicing programs. *Nat. Neurosci.* **22**, 1709–1717 (2019).

18. Olsen, R. H. J. *et al.* TRUPATH, an open-source biosensor platform for interrogating the GPCR transducerome. *Nat. Chem. Biol.* **16**, 841–849 (2020).

19. Sadler, F. *et al.* Autoregulation of GPCR signalling through the third intracellular loop. *Nature* (2023) doi:10.1038/s41586-023-05789-z.

20. Harada, K. *et al.* Red fluorescent protein-based cAMP indicator applicable to optogenetics and in vivo imaging. *Sci. Rep.* **7**, 7351 (2017).

21. Ovando-Zambrano, J. C., Arias-Montaño, J. A. & Boucard, A. A. Alternative splicing event modifying ADGRL1/latrophilin-1 cytoplasmic tail promotes both opposing and dual cAMP signaling pathways. *Ann. N. Y. Acad. Sci.* **1456**, 168–185 (2019).

22. Pederick, D. T. *et al.* Context-dependent requirement of G protein coupling for Latrophilin-2 in target selection of hippocampal axons. *Elife* **2**, 1–52 (2023).

23. Brogna, S. & Wen, J. Nonsense-mediated mRNA decay (NMD) mechanisms. *Nat. Struct. Mol. Biol.* **16**, 107–113 (2009).

24. Sun, Z. & Südhof, T. C. A simple Ca2+-imaging approach to neural network analyses in cultured neurons. *J. Neurosci. Methods* **349**, 109041 (2021).

25. Wang, J. *et al.* RTN4/NoGo-receptor binding to BAI adhesion-GPCRs regulates neuronal development. *Cell* **184**, 5869-5885.e25 (2021).

26. Tobaben, S., Sudhof, T. C. & Stahl, B. The G protein-coupled receptor CL1 interacts directly with proteins of the shank family. *J. Biol. Chem.* **275**, 36204–36210 (2000).

27. Kreienkamp, H. J., Zitzer, H., Gundelfinger, E. D., Richter, D. & Bockers, T. M. The calcium-independent receptor for α-latrotoxin from human and rodent brains interacts with members of the ProSAP/SSTRIP/Shank family of multidomain proteins. *J. Biol. Chem.* **275**, 32387–32390 (2000).

28. Zeng, M. *et al.* Reconstituted Postsynaptic Density as a Molecular Platform for Understanding Synapse Formation and Plasticity. *Cell* **174**, 1172-1187.e16 (2018).

29. del Toro, D. *et al.* Structural Basis of Teneurin-Latrophilin Interaction in Repulsive Guidance of Migrating Neurons. *Cell* **180**, 323-339.e19 (2020).

30. Li, J. *et al.* Alternative splicing controls teneurin-latrophilin interaction and synapse specificity by a shape-shifting mechanism. *Nat. Commun.* **11**, (2020).

31. Li, J. *et al.* Structural Basis for Teneurin Function in Circuit-Wiring: A Toxin Motif at the Synapse. *Cell* **173**, 735-748.e15 (2018).

32. Lu, Y. C. *et al.* Structural Basis of Latrophilin-FLRT-UNC5 Interaction in Cell Adhesion. *Structure* **23**, 1678–1691 (2015).

33. Seiradake, E. *et al.* FLRT Structure: Balancing Repulsion and Cell Adhesion in Cortical and Vascular Development. *Neuron* **84**, 370–385 (2014).

34. Pollina, E. A. *et al.* A NPAS4–NuA4 complex couples synaptic activity to DNA repair. *Nature* **614**, 732–741 (2023).

35. Mao, W. *et al.* Activity-Induced Regulation of Synaptic Strength through the Chromatin Reader L3mbtl1. *Cell Rep.* **23**, 3209–3222 (2018).

36. Liakath-Ali, K. & Südhof, T. C. The Perils of Navigating Activity-Dependent Alternative Splicing of Neurexins. *Front. Mol. Neurosci.* **14**, 1–19 (2021).

37. Chen, M. B., Jiang, X., Quake, S. R. & Südhof, T. C. Persistent transcriptional programmes are associated with remote memory. *Nature* **587**, 437–442 (2020).

38. Dana, H. *et al.* Sensitive red protein calcium indicators for imaging neural activity. *Elife* **5**, e12727 (2016).

39. Bae, S., Park, J. & Kim, J. S. Cas-OFFinder: A fast and versatile algorithm that searches for potential off-target sites of Cas9 RNA-guided endonucleases. *Bioinformatics* (2014) doi:10.1093/bioinformatics/btu048.

40. Tasic, B. *et al.* Shared and distinct transcriptomic cell types across neocortical areas. *Nature* **563**, 72–78 (2018).

41. Miyamichi, K. *et al.* Dissecting local circuits: Parvalbumin interneurons underlie broad feedback control of olfactory bulb output. *Neuron* **80**, 1232–1245 (2013).

42. Van Der Walt, S. *et al.* Scikit-image: Image processing in python. *PeerJ* (2014) doi:10.7717/peerj.453.

43. Koch, E. W. & Rosolowsky, E. W. Filament identification through mathematical morphology. *Mon. Not. R. Astron. Soc.* (2015) doi:10.1093/mnras/stv1521.

44. Brown, B. L. *et al.* CaImAn an open source tool for scalable calcium imaging data analysis. *Elife* **8**, (2019).

45. Virtanen, P. *et al.* SciPy 1.0: fundamental algorithms for scientific computing in Python. *Nat. Methods* (2020) doi:10.1038/s41592-019-0686-2.

46. Franklin, K. & Paxinos, G. Paxinos and Franklin's the Mouse Brain in Stereotaxic Coordinates, Compact. in *Academic Press* (2019).

47. Platt, R. J. *et al.* CRISPR-Cas9 knockin mice for genome editing and cancer modeling. *Cell* **159**, 440–455 (2014).

48. Anderson, G. R. *et al.* Postsynaptic adhesion GPCR latrophilin-2 mediates target recognition in entorhinal-hippocampal synapse assembly. *J. Cell Biol.* **216**, 3831–3846 (2017).

49. Araç, D. *et al.* A novel evolutionarily conserved domain of cell-adhesion GPCRs mediates autoproteolysis. *EMBO J.* **31**, 1364–1378 (2012).

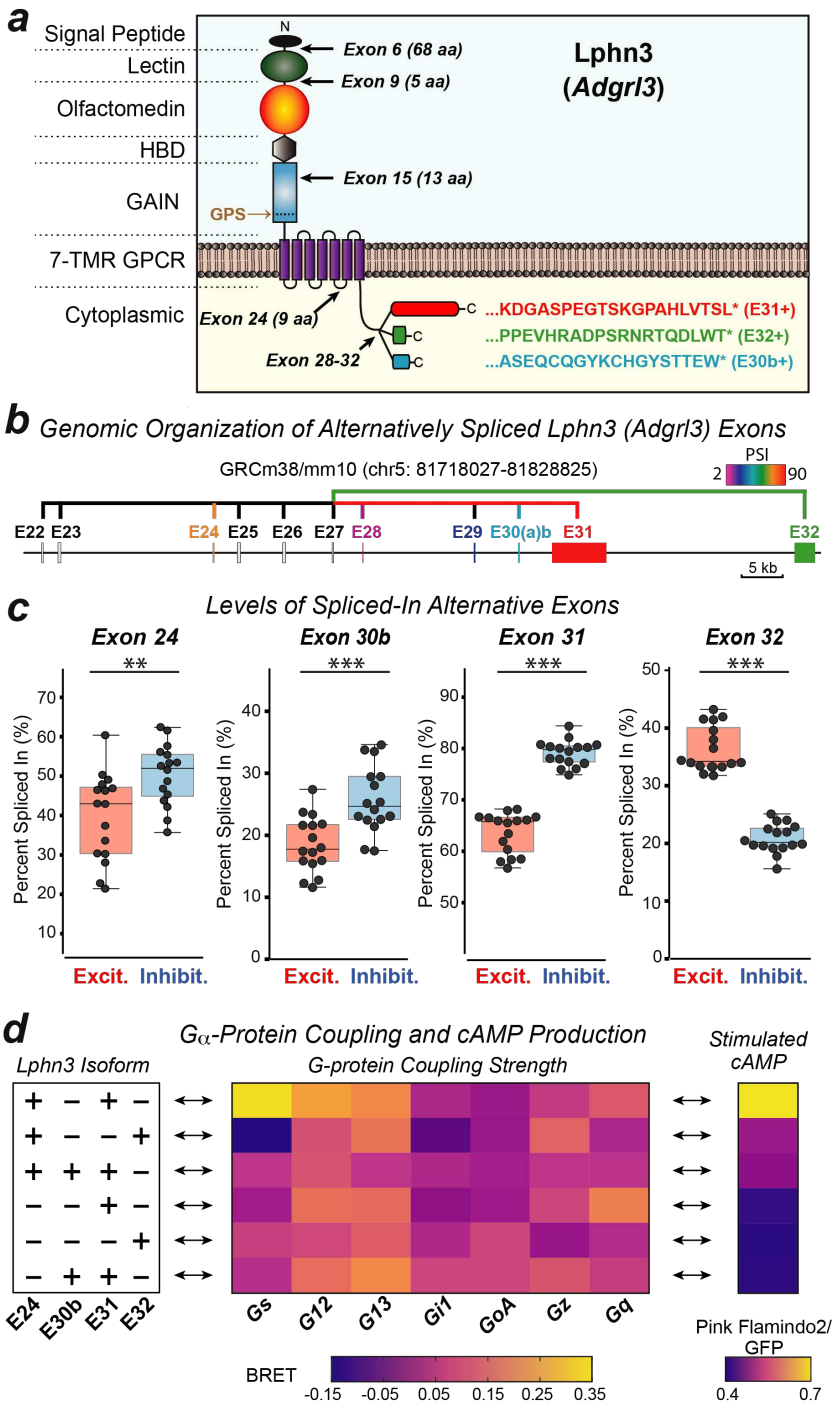

Figure 1: Differentially expressed Lphn3 (*Adgrl3*) splice variants couple to different G proteins

a, Schematic of Lphn3 alternative splicing (asterisk = stop codon).

b, Genomic organization of the 3' alternatively spliced exons of the Lphn3 gene. Alternative exons are color-coded based on percent spliced-in (PSI) in hippocampus (ED Fig 1c), with constitutive exons colored gray.

c, Cell type-specific splicing of Lphn3. Raw data from ribosome-associated transcriptome analyses[17] were analyzed to calculate the percent spliced-in (PSI) of each exon for excitatory and inhibitory

neurons (for subtype-specific data, see ED Figure 1c). Each datapoint represents one sample (n=16). Two-sided Student's t-test was used to calculate the statistical significance (**p < 0.01; ***p < 0.001).

d, G-protein coupling and stimulated cAMP levels associated with Lphn3 splice variants (left, splice variants; middle, G-protein coupling signal (BRET signal) from TRUPATH assays; right, cAMP stimulated by Lphn3 splice variant expression in HEK293 cells). For detailed data, see ED Figure 4 and 5a.

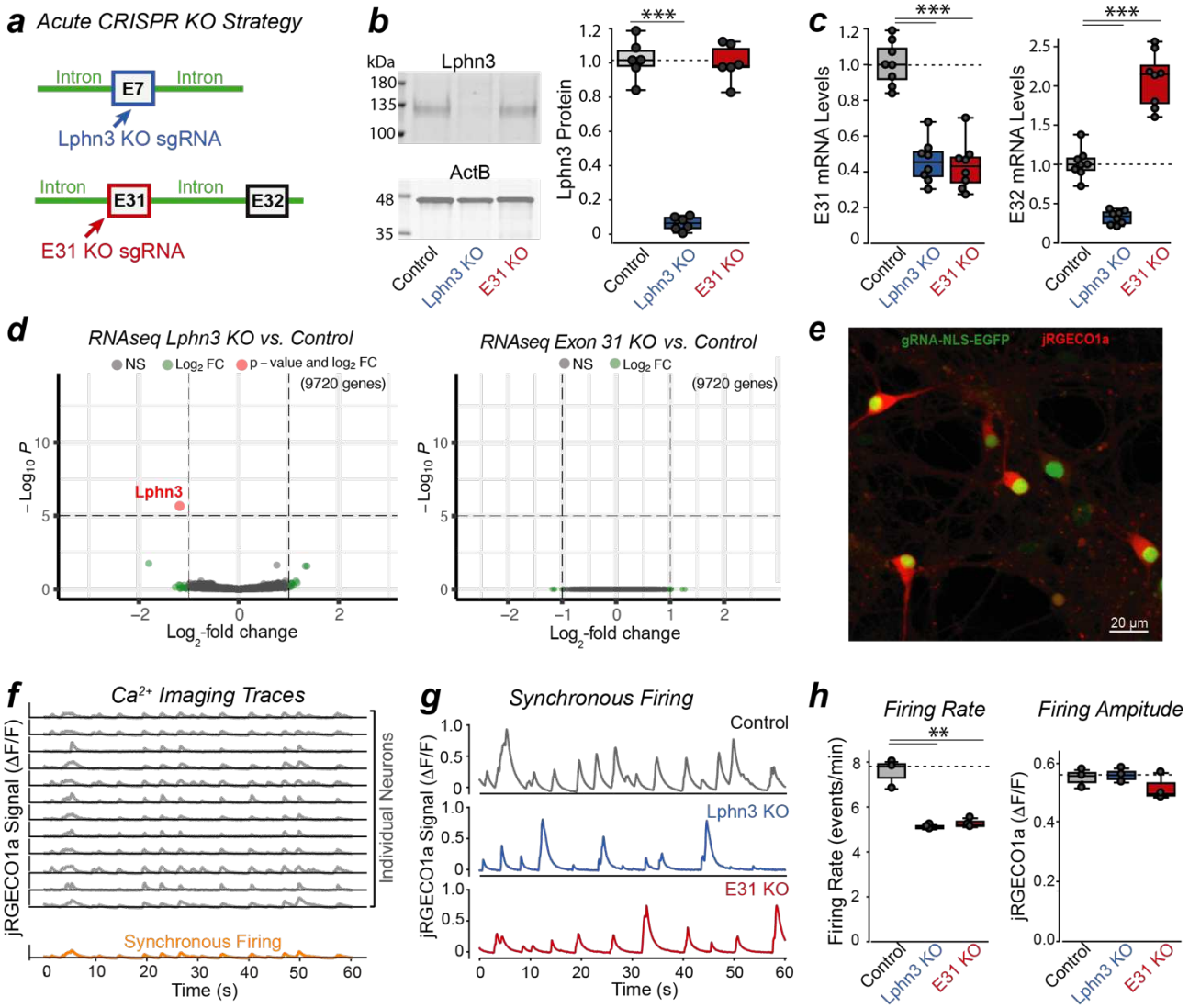

Figure 2: CRISPR-mediated conversion of Lphn3 alternative splicing from Exon31 to Exon32 impairs neuronal network activity

a, CRISPR strategy producing either an acute deletion of Lphn3 expression (Lphn3 KO) or a selective deletion of Exon31 (E31 KO) of Lphn3.

b, Lphn3 immunoblots showing that the acute Exon31-specific KO (E31 KO) does not change Lphn3 protein levels, whereas the Lphn3 KO ablates Lphn3 expression. Hippocampal cultures were subjected to CRISPR at DIV3 using lentiviral delivery and analyzed at DIV14 (control = CRISPR with non-targeting gRNA). Each data point represents one independent culture (n=6); two-sided Student's t-test was used to calculate the statistical significance (***p < 0.001).

c, Quantitative RT-PCR (RT-qPCR) measurements demonstrating that the E31 KO and the Lphn3 KO similarly ablate expression of Exon31-containing Lphn3 mRNAs (left) but have opposite effects on Exon32-containing Lphn3 mRNAs (right). Exon31 or Exon32 junctions with the constitutive Exon 27 were PCR amplified, Ct values were normalized to β actin and all ΔCt values were normalized to

controls. Each data point represents one independent culture (n=8); two-sided Student's t-test was used to calculate the statistical significance (***p < 0.001).

d, RNAseq analyses of differentially expressed genes shown in volcano plots, by comparing Lphn3 KO to control (left), or Lphn3 Exon31-specific KO to control (right). All data were from 3 independent cultures. Note that only a single gene (Lphn3, the target) has significantly decreased expression by Lphn3 KO, and that no genes were significantly perturbed by Lphn3 Exon31-specific KO.

e, Representative Ca^{2+}-imaging experiment of hippocampal neurons that were infected by lentiviruses expressing a gRNA, EGFP and jRGECO1a[38]. Green dots mark the nuclei of cells that were infected with the lentiviruses expressing the gRNA together with nuclear EGFP. The red signal of the soma corresponds to the jRGECO1a peak signal during a recording period.

f, Representative illustration of the extraction of jRGECO1a signals for individual neurons (gray, top) whose average is the synchronous firing trace for one field of view (orange, bottom).

g, Representative traces of synchronous firing of neurons analyzed in control, Lphn3 KO and E31 KO neurons for one field of view.

h, Quantification of synchronous firing rate (left) and amplitude (right) of Ca^{2+}-imaging signals. Each datapoint represents one independent culture (n=3); two-sided Student's t-test was used to calculate the statistical significance (**p < 0.01).

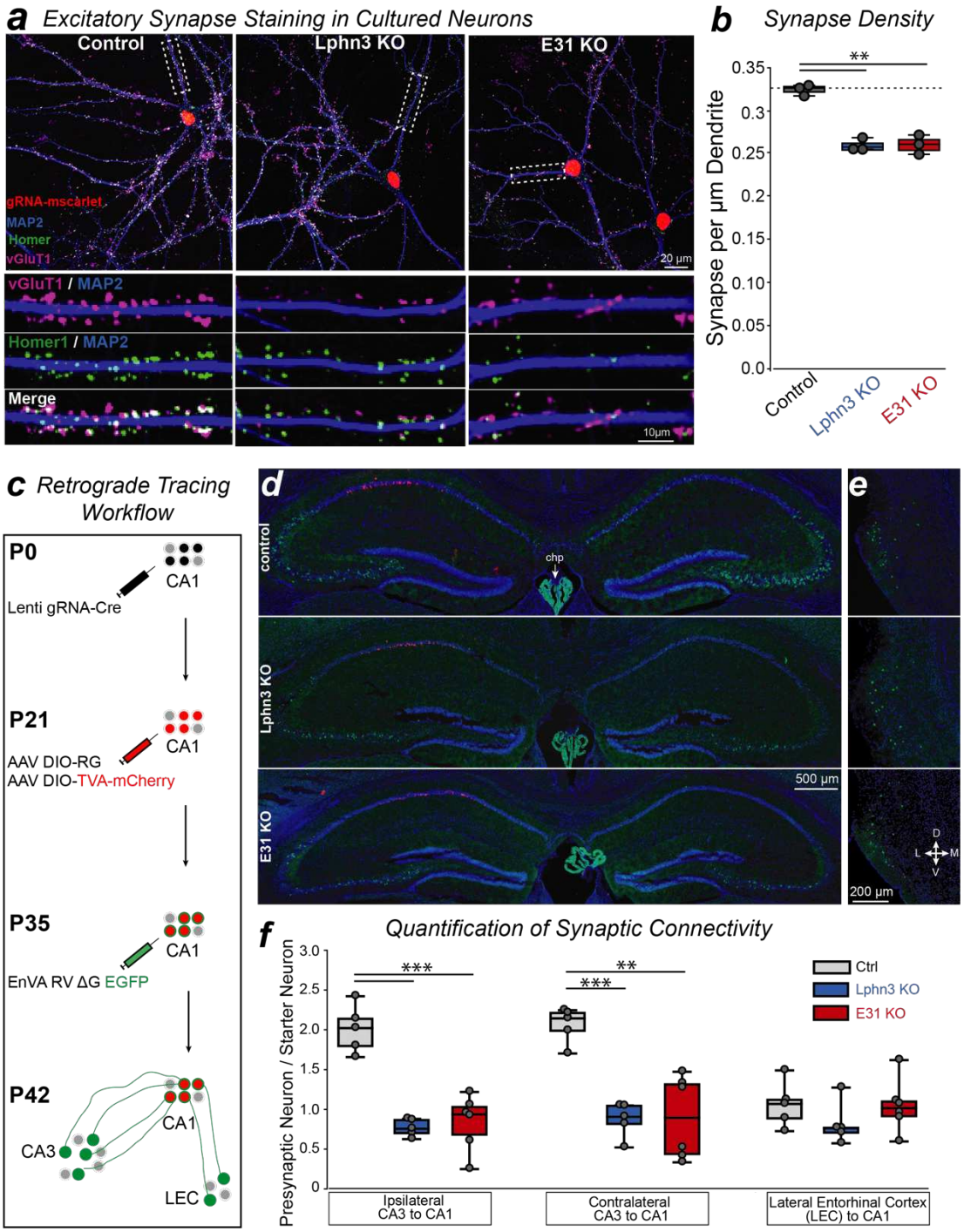

<u>Figure 3</u>: Switching Lphn3 G-protein coupling from $G_{\alpha S}$ to $G_{\alpha 12/13}$ by deleting Exon31 suppresses synaptic connectivity of hippocampal neurons

a & **b**, Selective deletion of Lphn3 Exon31 decreases the excitatory synapse density similarly to the entire deletion of Lphn3 (**a**, representative images of cultured hippocampal neurons stained with antibodies to vGluT1, Homer1 and MAP2; **b**, summary graph of the density of puncta that were positive for both vGluT1 and Homer1). Hippocampal cultures from CAG-Cas9 mice[47] were transduced with lentiviruses expressing gRNA and nuclear-localized mScarlet-I at DIV3 and

analyzed at DIV14. Each datapoint represents an independent culture (n=3); two-sided Student's t-test was used to calculate statistical significance (**p < 0.01).

c, Experimental strategy for the retrograde tracing of monosynaptic connections using pseudo-typed rabies virus[41,4] in CA1 neurons with acute CRISPR-mediated in vivo deletions of Lphn3 or Exon31 of Lphn3.

d & **e**, Representative images of pseudo-typed rabies tracing experiments in the hippocampal region (**d**) and Lateral Entorhinal Cortex (LEC) (**e**). Note the weak GFP signal from the Cas9 mice is observed in the dentate gyrus granule cells and choroid plexus (chp), but not in CA3 pyramidal cells (ED Figure 5e).

f, Acute CRISPR-mediated in vivo deletion of Exon31 of Lphn3 (Lphn3 E31 KO) impairs the number of CA3-region input synapses in CA1-region neurons to a similar extent as the overall deletion of Lphn3 (Lphn3 KO) as quantified by retrograde pseudo-typed rabies virus tracing. Box plots show the number of presynaptic neurons (ipsilateral CA3, contralateral CA3, and ipsilateral LEC) normalized to the starter neuron number. Each datapoint represents one animal (n=5-6); two-sided Student's t-test was used to calculate statistical significance (**p < 0.01; ***p < 0.001). Note that the Lphn3 E31 KO and the Lphn3 KO do not affect entorhinal cortex input synapses which depend on Lphn2 instead of Lphn3[4,48].

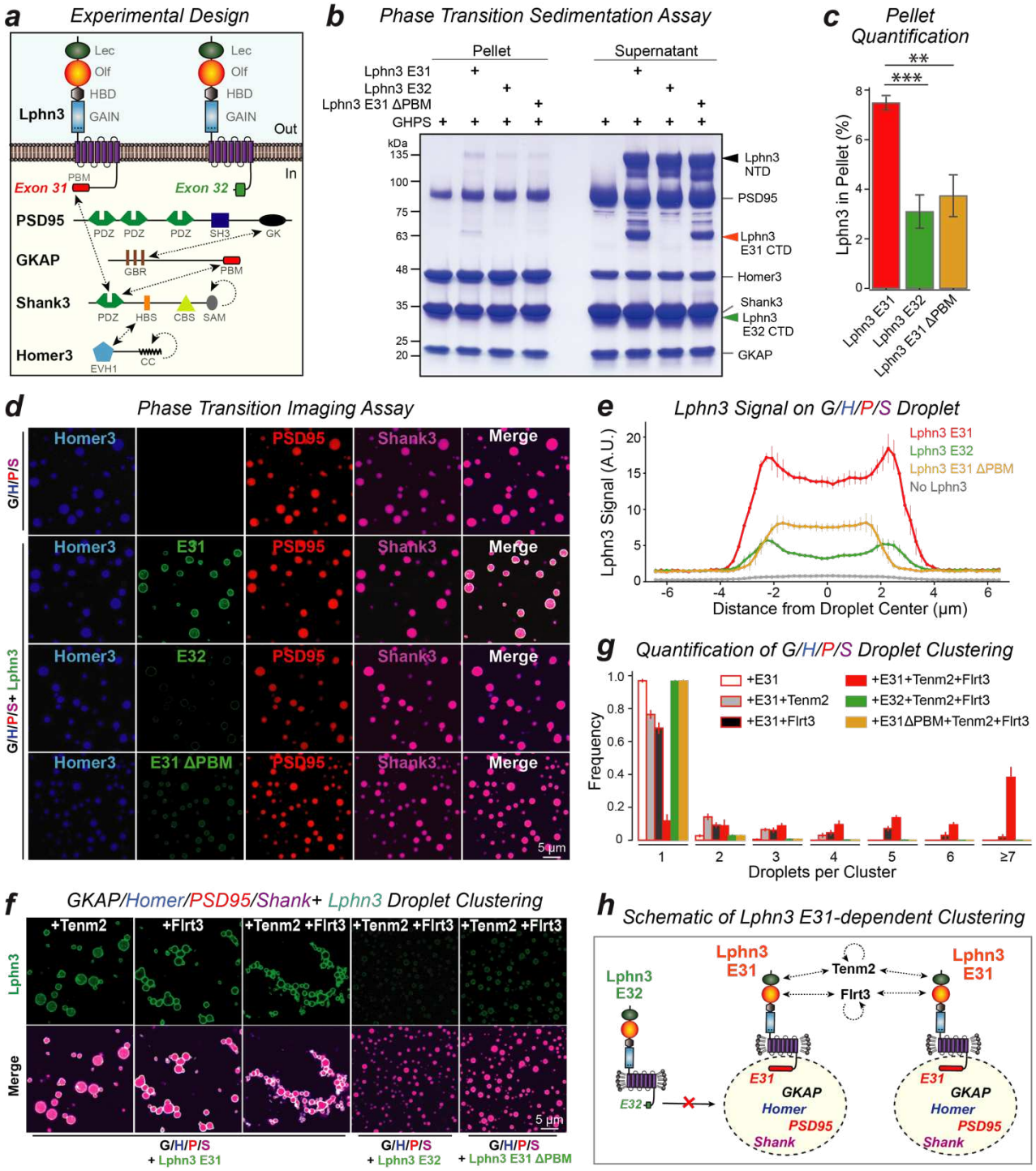

Figure 4: The alternatively spliced Lphn3 variant containing Exon31 but not the variant containing Exon32 spontaneously incorporates into phase-separated assemblies formed by postsynaptic scaffold proteins

a, Schematic of proteins (dashed arrows, interactions; circling arrows, homo-oligomerizations; Lec: lectin-like domain, Olf: olfactomedin-like domain, HBD: hormone-binding domain, PBM: PDZ-binding

motif, GK: guanylate kinase domain, GBR: GK binding repeat, HBS: Homer-binding sequence, CBS: cortactin-binding sequence, CC: coiled-coil). Note PSD95 and Homer3 are full-length constructs, whereas GKAP and Shank3 are truncated constructs to obtain soluble proteins.

b, Sedimentation assay of phase transition complexes. The scaffold protein mixture containing GKAP, Homer3, PSD95, and Shank3 (GHPS) was incubated with indicated Lphn3. Pellet and supernatant were separated by centrifugation and analyzed by SDS-PAGE. Lphn3 is autocleaved at GPS site to produce N-terminal (NTD, black arrow) and C-terminal domains (CTD, red and green arrow)[49] (see ED Figure 6). The Lphn3 Exon32 CTD fragments migrates similarly to Shank3. See New Extended Data Figure 6j. Thus we quantify the Lphn3 pellet % using the NTD which has the same sequence for all three Lphn3 constructs.

c, Quantification of Lphn3 pelleting in the sedimentation assay. The bands corresponding to the Lphn3 NTD were the same for all three Lphn3 constructs and used for analysis. Barplot shows the mean ± SEM (n=4 independent experiments). Two-sided Student's t-test was used to calculate the statistical significance (**$p < 0.01$, ***$p < 0.001$).

d, Imaging of phase transitioned complexes. Homer3 (H), Lphn3 (E31, E32 and E31 ΔPBM), PSD95 (P), and Shank3 (S) were labeled by NHS-ester fluorophore 405, 488, 546, 647, respectively, while GKAP (G) was unlabeled.

e, Quantification of the Lphn3 across the phase-separated droplet illustrating the surface localization of Lphn3 E31 on the droplet. Data are means ± SEM (n = 3 independent experiments). Also see ED Figure 7d, 8a.

f, Representative images of phase-transitioned postsynaptic scaffold protein complexes containing Lphn3 E31 that were clustered by presynaptic ligands Tenm2 and Flrt3.

g, Quantification of the clustering effect of presynaptic Tenm2 and Flrt3 ligands on Lphn3 E31 coated, phase-transitioned postsynaptic scaffolding protein complexes. Data are means ± SEM (n = 3 independent experiments).

h, Schematic of the localization of Lphn3 E31 but not of Lphn3 E32 on the surface of phase-transitioned droplets formed by post-synaptic scaffold proteins, and the clustering of droplets by Lphn3 ligands Tenm2 and Flrt3. Dashed arrows, interactions; circling arrows, homo-oligomerizations.

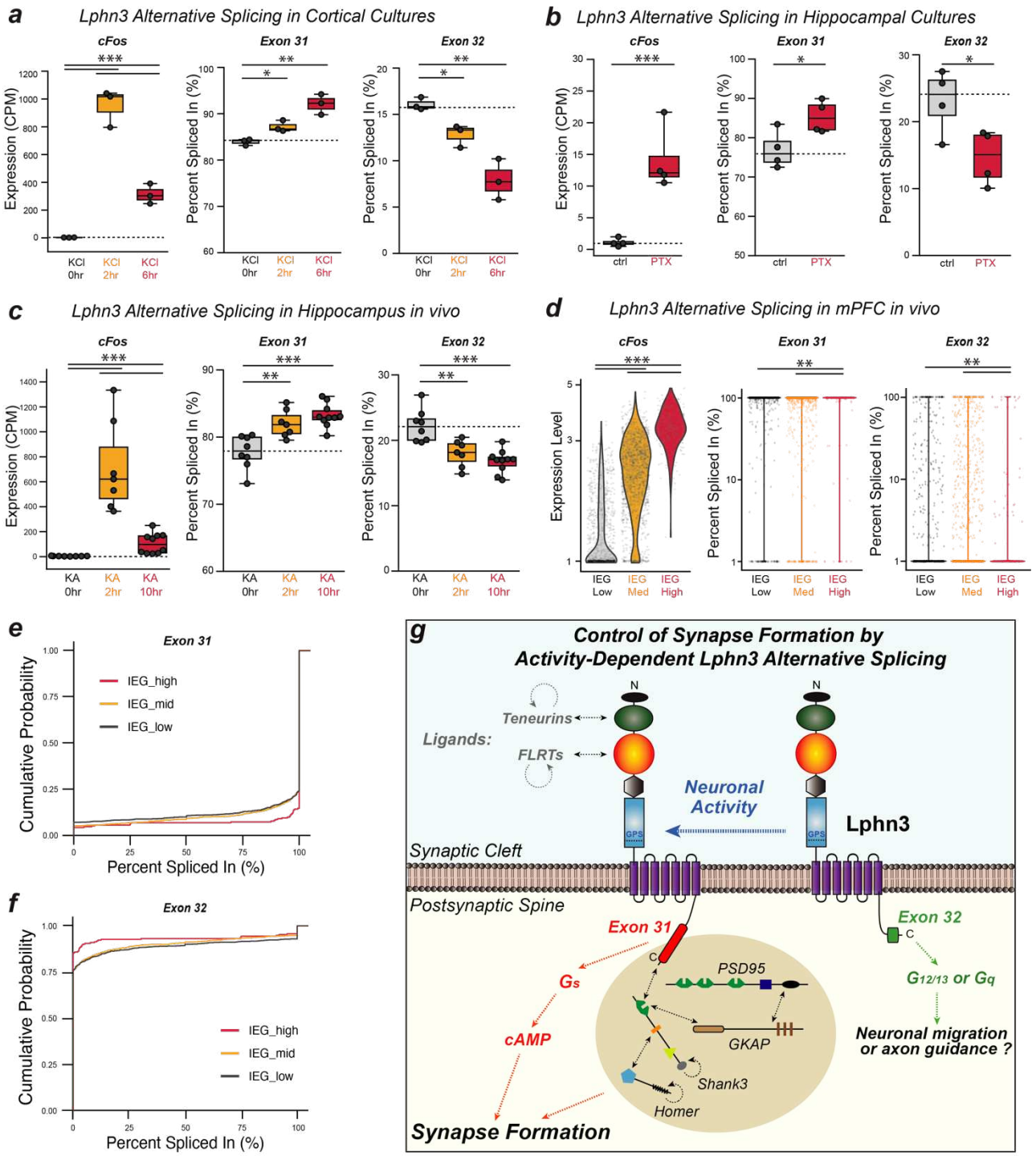

Figure 5: Neuronal activity promotes Exon31 inclusion and Exon32 exclusion in Lphn3 by alternative splicing, leading to increased expression of the synaptogenic Lphn3-Exon31 splice variant

a-c, Elevated neuronal activity (cFos as marker) induced by KCl-depolarization in primary cortical cultures[34] (a), blocking GABA receptor using picrotoxin in primary hippocampal cultures[35] (b), and hippocampus tissue after in vivo kainate injections[34] (c). The percent-spliced in for Exon31 and Exon32 of Lphn3 is shown for each treatment. Each datapoint represents one replicate (n=3-7). Two-

sided Student's t-test was used to calculate statistical significance for percent spliced-in. Wilcoxon rank-sum test was used to calculate the statistical significance of total gene expression (*p < 0.05; **p < 0.01; ***p < 0.001).

d-f, Exon31 and Exon32 splicing in natively activated neurons from mPFC region[37]. Single neurons are classified to IEG low (903 cells), medium (1526 cells) and high (232 cells) group based on the expression level of activity marker genes (see ED Figure10d and Method). Each group plots the percent spliced-in of Exon31 (d, middle panel) or Exon32 (e, right panel) for individual neurons, and the cumulative probability of all neurons for Exon31 (e) or Exon32 (f). Wilcoxon rank-sum test was used to test the statistical significance (n.s, not significant; **p < 0.01; ***p < 0.001).

g, Model of the mechanism of action of Lphn3 in synapse formation and the regulation of Lphn3 function by alternative splicing of Exon31.

Extended Data Figures and Figure Legends

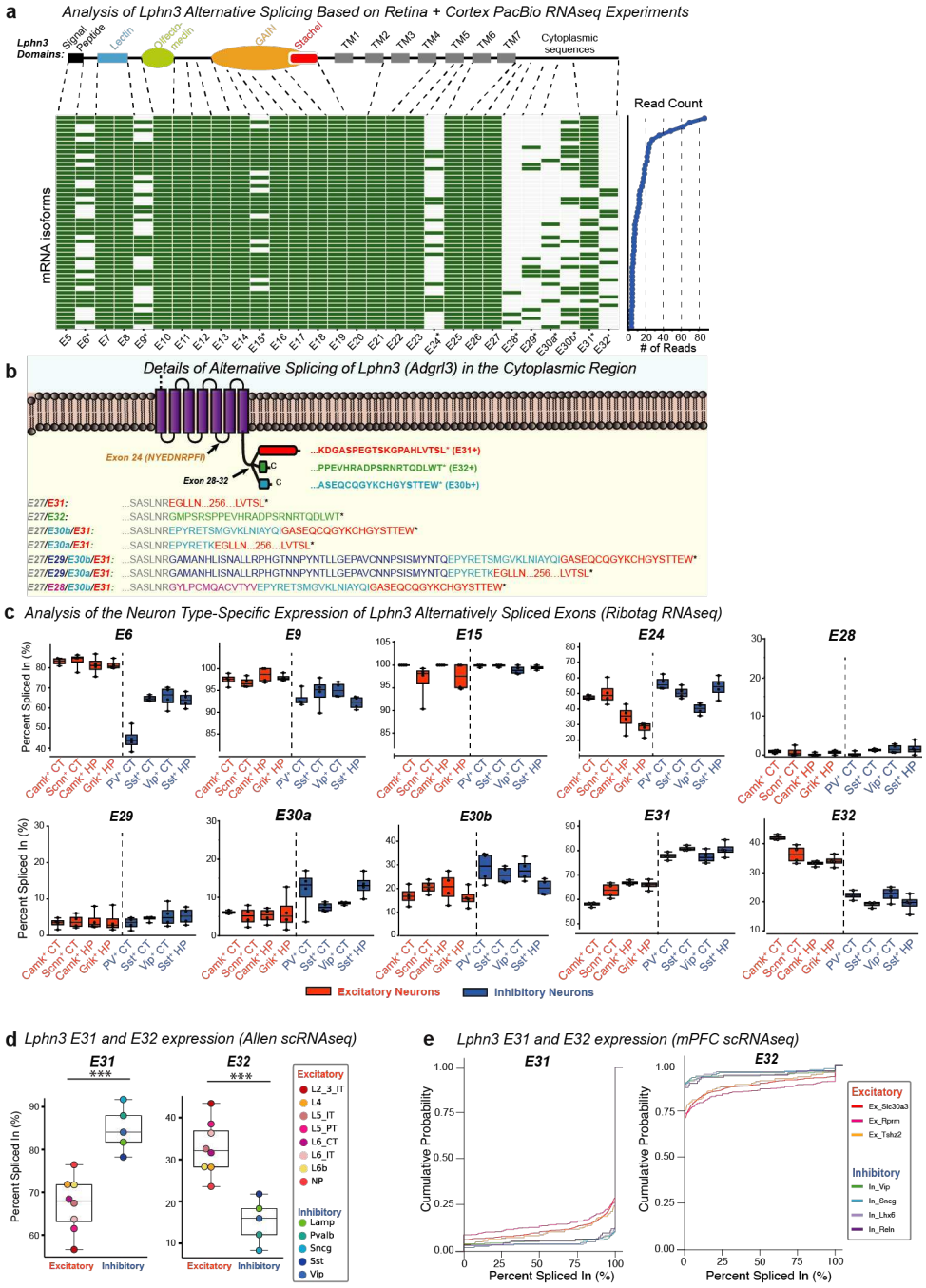

Extended Data Figure 1: Alternative splicing of Lphn3 (*Adgrl3*) transcripts (*a* & *b*) and demonstration that a subset of the sites of alternative splicing of Lphn3 exhibits a high degree of cell-type specificity as revealed by RNAseq analyses (*c*-*e*)

a, Analysis of a long-read PacBio sequencing data set from retina and cortex (NCBI BioProject repository; accession number PRJNA547800)[1] uncovers extensive combinatorial alternative splicing of Lphn3 mRNAs. Reads are depicted as heatmaps (green boxes = Included exons; light gray boxes = excluded exons; exon numbers with asterisks = alternatively spliced exon). Each row represents a splice variant combination whose abundance is shown on the right (only the top 50 variants are

shown). Note that for this figure and all following figures, ‘a’ and ‘b’ designations (such as ‘30a’ and ‘30b’) are alternative splicing donor or acceptor variants within an exon (see method “Generation of reference exon list” for details). For a similar analysis of Lphn2 and Lphn3, see ED Figure 2c, d.

b, Detailed schematic of alternative splicing in the cytoplasmic region of Lphn3. The diagram depicts the amino acid sequence changes of alternatively spliced variants (asterisk = stop codon; only the 7 TMR region and cytoplasmic sequences of Lphn3 are shown). Note that whereas inclusion of the low-abundance exons E28, E29, and E30a introduces additional diversity, only three principal C-terminal Lphn3 sequence variants exist that are encoded by: (1) Exon 31 without the low-abundance Exon 30b, (2) Exon 31 with the low-abundance Exon 30b, and (3) Exon 32.

c, Neuron type-specific alternative splicing of Lphn3. Raw data from a ribosome-associated transcriptome study[2] were analyzed to calculate the abundance of each exon in PSI (percent spliced in) for 8 indicated neuron types from two brain regions (HP: hippocampus, CT: cortex). Each datapoint (n=4) represents one sample from 1 animal for excitatory neurons, and 2 animals for inhibitory neurons. The distribution of datapoints are shown in boxplots.

d & e, Analyses of Lphn3 Exon31 and Exon32 level in single-cell datasets from primary visual cortex and anterior lateral motor cortex[3] (*d*), or of medial prefrontal cortex[4] (*e*). In *d*, all neurons corresponding to an indicated type were compiled as one datapoint. The percent spliced-in for Exon31 and Exon32 of Lphn3 is shown for each type. Two-sided Student’s t-test was used to calculate statistical significance (***$p < 0.001$). In *e*, the cumulative probability of splicing percentage for all neurons of each type were plotted.

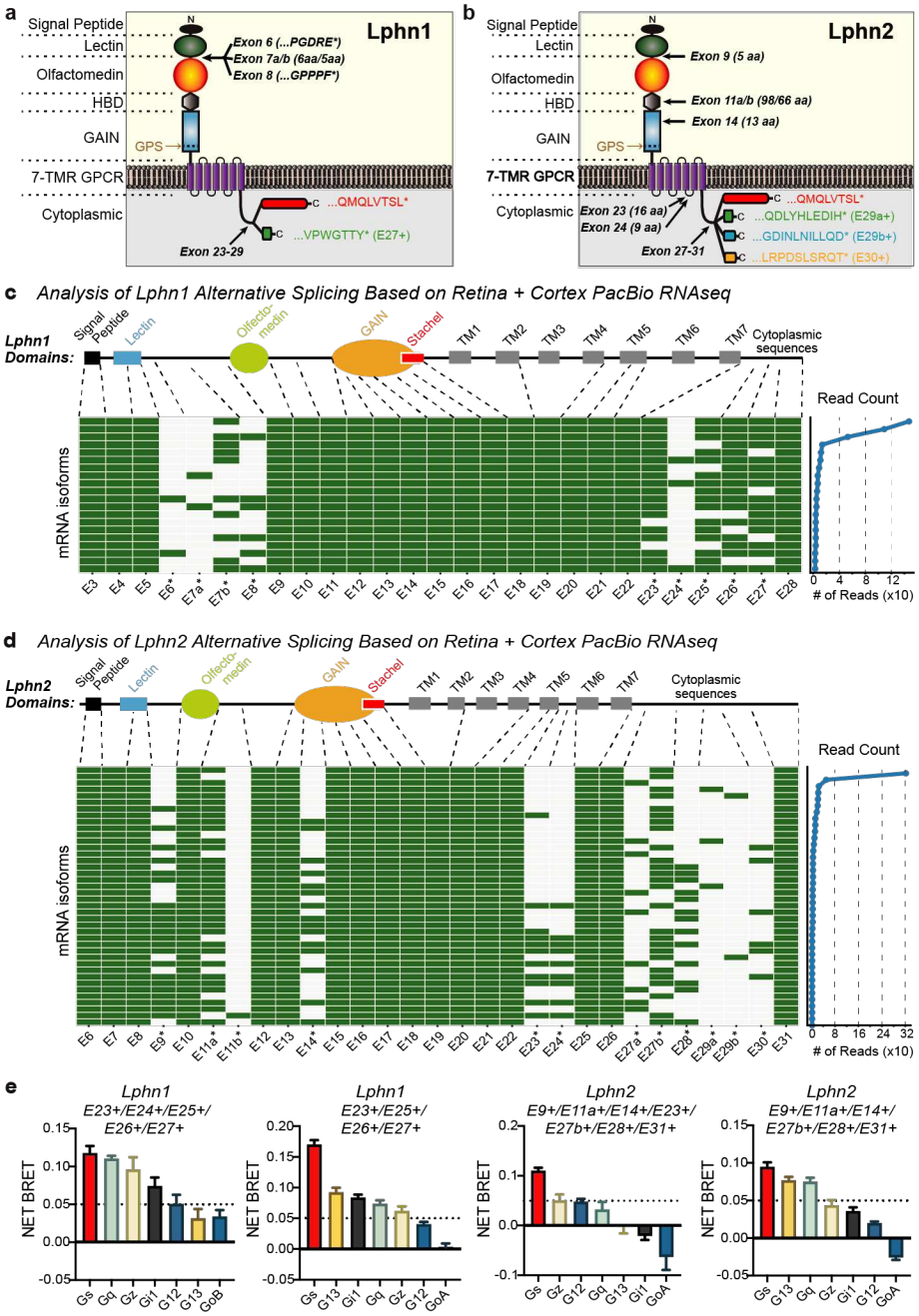

Extended Data Figure 2: Regulation of G-protein coupling by alternative splicing of Lphn1 (*Adgrl1*) and Lphn2 (*Adgrl2*)

a & **b**, Schematic of Lphn1 (*Adgrl1*) (a) and Lphn2 (*Adgrl2*) (b) alternative splicing with a depiction of the amino acid sequences of some of the resulting variants (asterisk = stop codon).

c & **d**, Analysis of a long-read PacBio sequencing dataset from retina and cortex (NCBI BioProject repository; accession number PRJNA547800)[1] also reveals extensive combinatorial alternative splicing of Lphn1 and Lphn2 mRNAs. Reads are depicted as heatmaps (green boxes = Included

exons; light gray boxes = excluded exons; exon numbers with asterisks = alternatively spliced exon). Each row represents a splice variant combination whose abundance is shown on the right (only the most abundant variants are shown).

e, G-protein coupling preferences of two Lphn1 and Lphn2 splice variants revealed by TRUPATH analyses. The constitutive G-protein coupling strength (represented by the NET BRET signal) of the indicated Lphn1 and Lphn2 isoform were measured by TRUPATH assay in HEK293 cell. Splice variants with indicated spliced-in exons are shown. BRET signals at 300 ng receptor-transfected condition were normalized to the 0 ng transfected baseline. Graphs show means ± SEM from three batches of experiments (n=3).

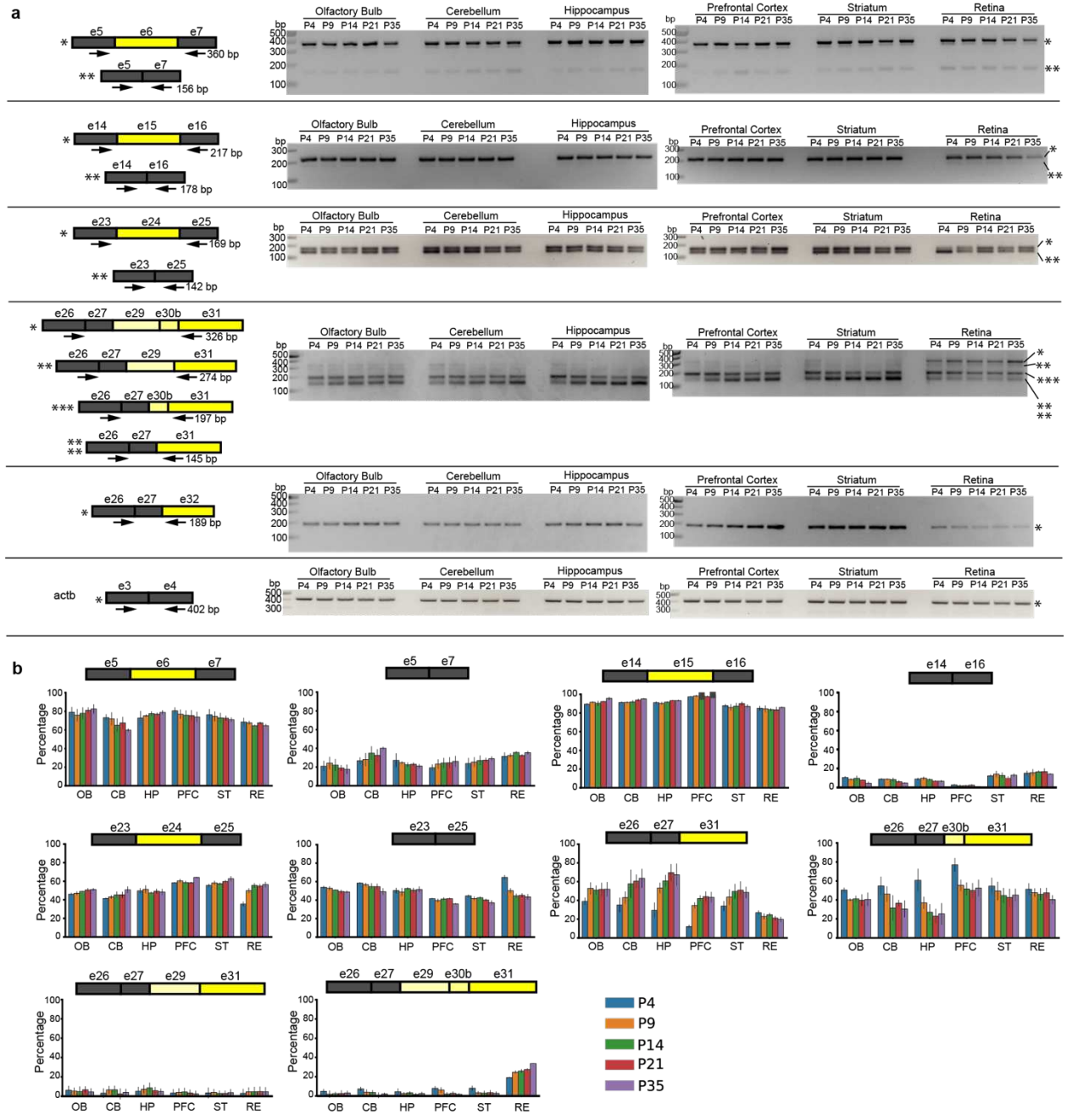

<u>Extended Data Figure 3</u>: Diverse patterns of Lphn3 alternative splicing analyzed by RT-PCR in different brain regions and at different times of postnatal development

a, Total RNA isolated from the indicated brain regions of C57BL/6 mice at the indicated postnatal developmental timepoints were analyzed by RT-PCRs using primers (labeled in arrows) at exon-exon junctions. RT-PCR products were separated by 2% agarose gel electrophoresis; bands are marked based on the predicted sizes of the alternatively spliced variants shown above each gel.

b, Quantification of the percentage of multiple variants derived from the same PCR primer pairs. Note Exon32 of Lphn3 and β-actin has only one product, therefore were not quantified.

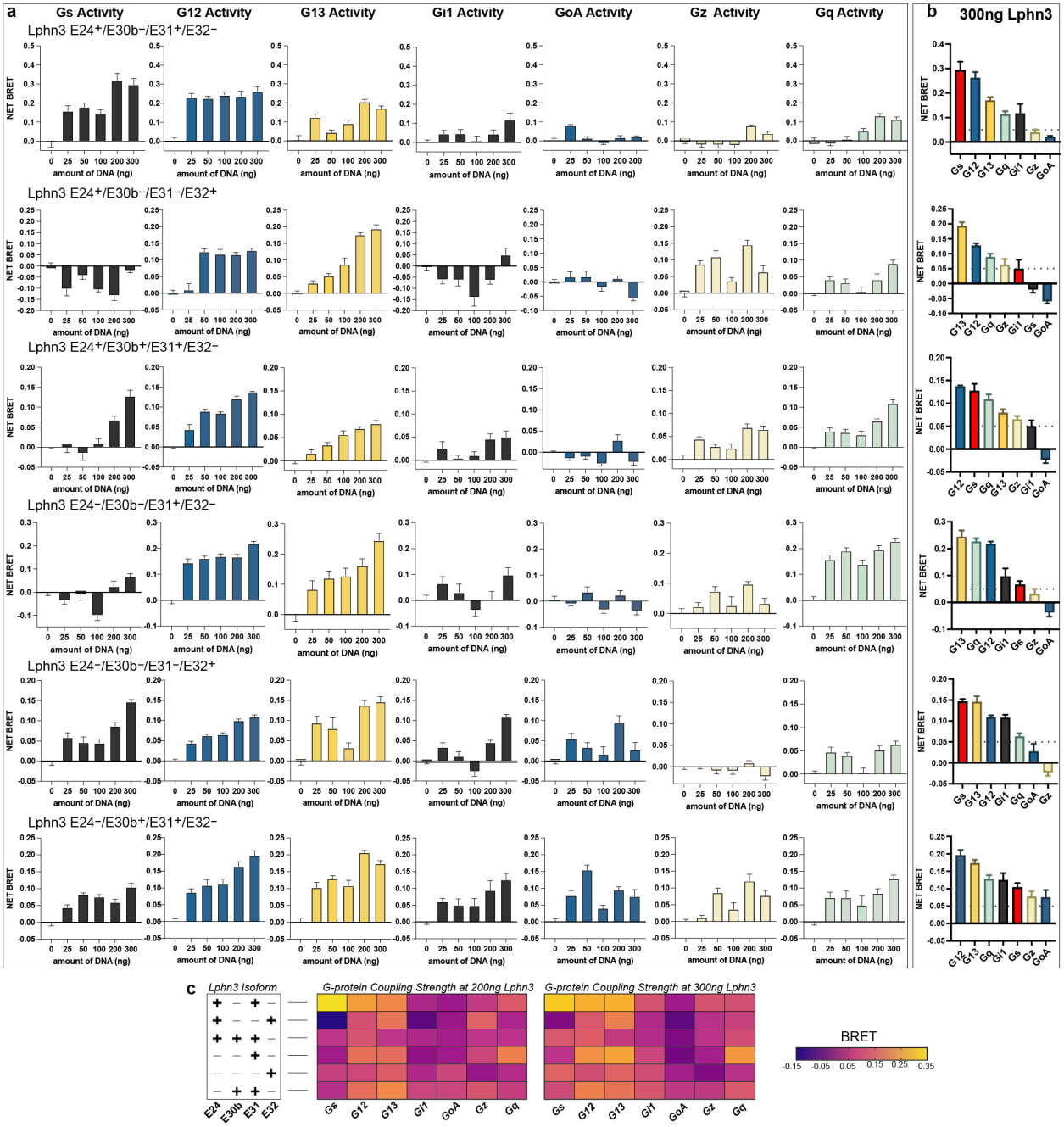

<u>Extended Data Figure 4</u>: Detailed TRUPATH analyses of G-protein coupling mediated by six different Lphn3 splice variants

a, TRUPATH assays reveal G-protein coupling signals (NET BRET values) mediated by 6 Lphn3 splice variants expressed at different concentrations. HEK293 cells were transfected with Lphn3 expression plasmids at concentrations of 0-300 ng and the TRUPATH signal was monitored as described. Graphs show means ± SEM from three independent experiments (n=3). All signals were normalized to 0 ng transfected baseline.

b, Summary graph of the TRUPATH signal at the highest Lphn3 concentration (300 ng). Graphs show means ± SEM from three independent experiments (n=3). All signals were normalized to 0 ng transfected baseline.

c, Heatmap plot of the G-protein coupling strength of the indicated Lphn3 variants at the 200 ng and 300 ng Lphn3 plasmid transfection condition.

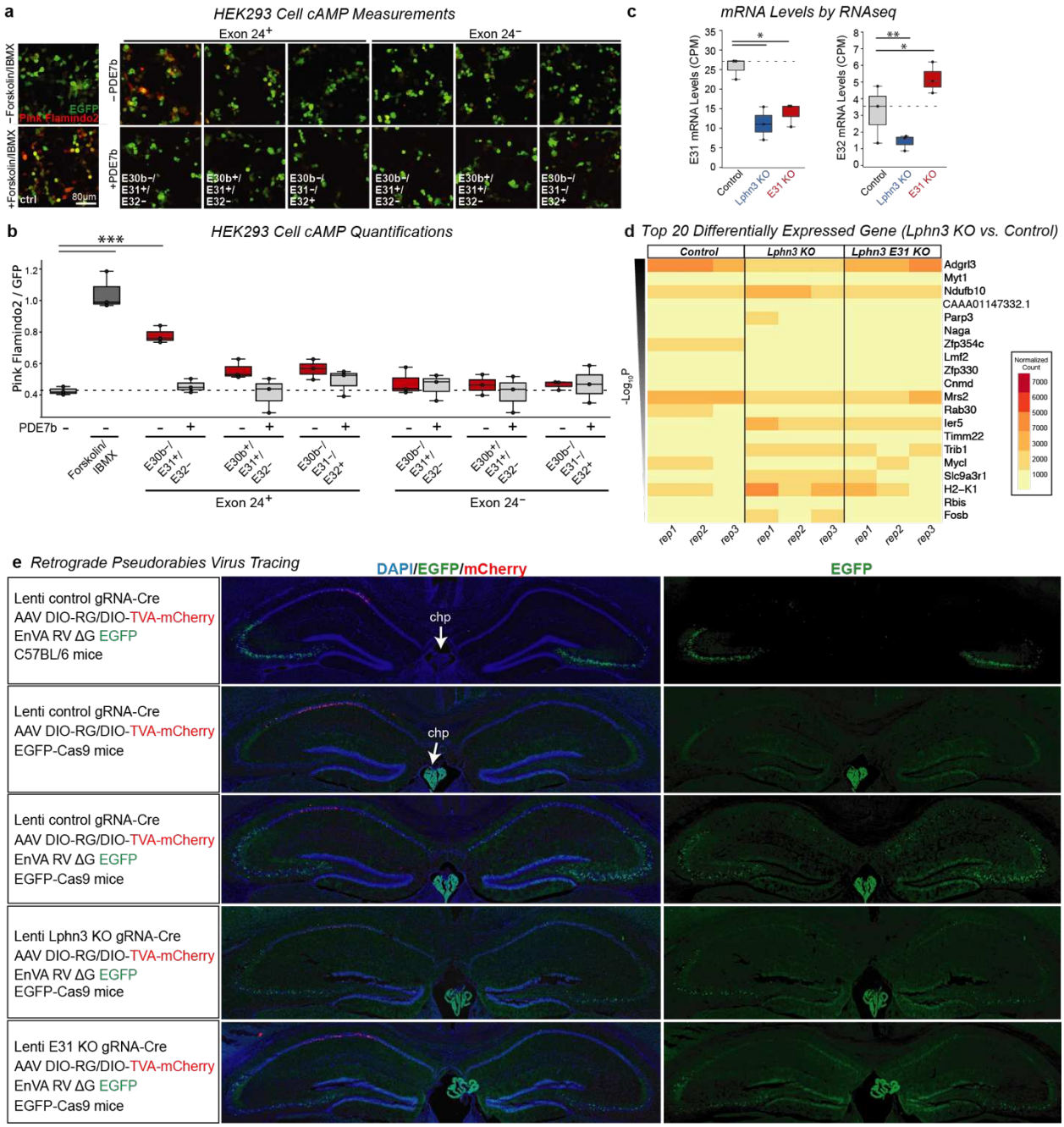

Extended Data Figure 5: Additional information for the cAMP assays, the RNAseq analyses and the pseudorabies virus tracing experiments

a, Representative images of the cAMP-dependent Pink Flamindo2 and the EGFP signal monitored during cAMP assays. Intracellular cAMP levels were monitored in live HEK293T cells that had been transfected with Pink Flamindo2, EGFP and Gs(α/β/γ). Where indicated, Lphn3 variants and/or PDE7b (a cAMP-specific phosphodiesterase that blocks cAMP signaling) were co-transfected. Forskolin/IBMX were only applied to the control group. Imaging was performed by 10x confocal microscopy.

b, Quantification of cAMP signals. The Pink Flamindo2 signal was normalized for the GFP signal in the same cells. Each datapoint represents one independent experiment (n = 3) as one batch of culture. Two-sided Student's t-test was used to calculate the statistical significance (***p < 0.001).

c, RNAseq confirm that the E31 KO and the Lphn3 KO similarly ablate expression of Exon 31-containing Lphn3 mRNAs (left) but have opposite effects on Exon 32-containing Lphn3 mRNAs (right). Each data point represents one independent culture (n=3). DEseq2 was used to calculate statistical significance (*p < 0.05; **p < 0.01).

d, Heatmap illustrating the most significant changes in gene expression observed in three independent RNAseq experiments (rep1-rep3). The normalized count of each replicate for each condition is shown for the top 20 genes which are differentially expressed (based on the p value of Lphn3 KO vs control).

e, Additional controls to illustrate the weak GFP signal present in Cas9 mice that is observed in dentate gyrus granule cells and in the choroid plexus (chp) but not in CA3 pyramidal cells (2nd row vs. 1st row).

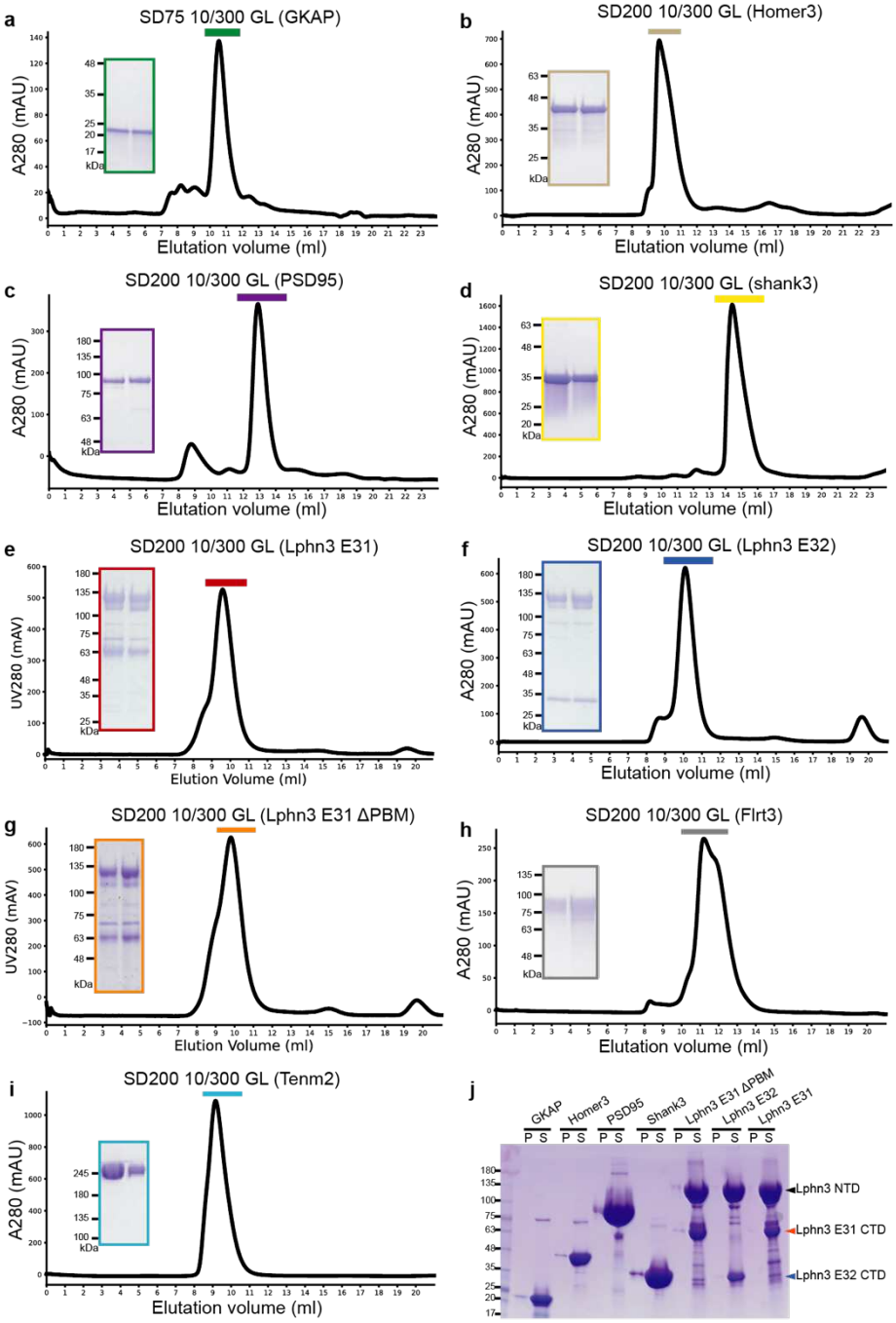

Extended Data Figure 6: Quality control of purified proteins used for phase-transition experiments

a-i, Chromatographs of proteins on size-exclusion columns during the last step of purification. Peak fractions were analyzed by SDS-PAGE and Coomassie staining (insets) and used as final purified proteins for phase separation experiments. Note that Lphn3 is autocleaved in the GAIN domain to produce N- (apparent molecular weight ~130 kD) and C-terminal fragments (apparent molecular weight ~65 kD for Lphn3-E31 and Lphn3-E31-ΔPBM, and ~30 kD for Lphn3-E32) which are non-covalently bound to each other within the GAIN domain[5].

j, Sedimentation behavior of individual proteins. Purified proteins were diluted to the same concentration, and centrifuged in the same condition, as used in the phase-transition assay. Supernatant (S) and pellet (P) were subject to SDS-PAGE for analysis. The concentrations of proteins used were: 80 μM GKAP, 100 μM PSD95, 80 μM Homer3, 200 μM Shank3, 40 μM Lphn3-E31 ΔPBM, 40 μM Lphn3-E32, and 40 μM Lphn3-E31.

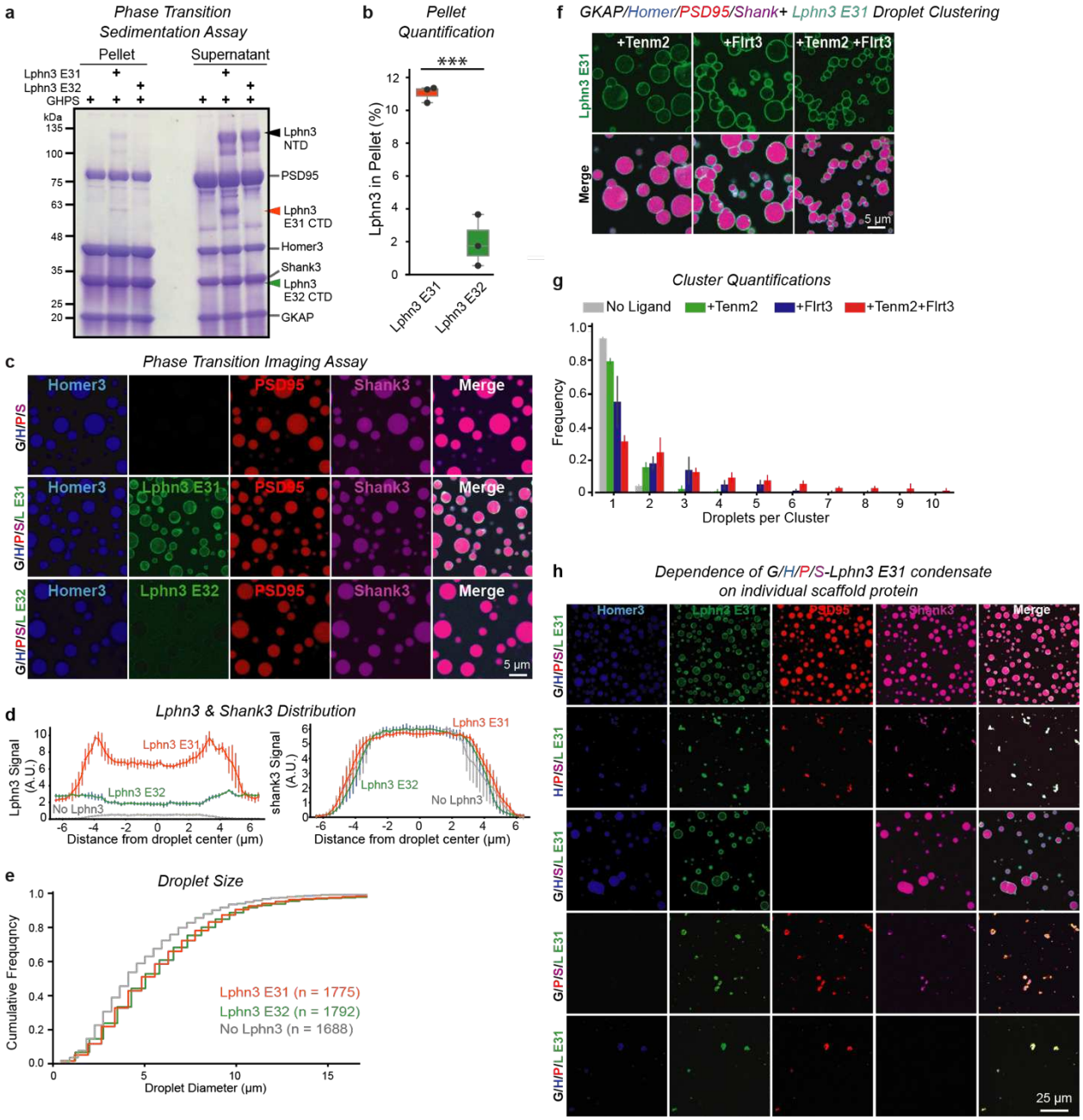

<u>Extended Data Figure 7</u>: Independent replication of the Lphn3-E31 dependent recruitment of phase-separated scaffold proteins at higher concentrations of scaffold proteins

a, Sedimentation assay of phase transition complexes. The scaffold protein mixture containing GKAP, Homer3, PSD95, and Shank3 (GHPS) was incubated with indicated Lphn3 proteins in detergent. Pellet and supernatant were separated by centrifugation and analyzed by SDS-PAGE.

b, Quantification of Lphn3 pelleting in the sedimentation assay. The bands corresponding to the Lphn3 NTD were used for analysis. Each datapoint represents one independent experiment (n=3); two-sided Student's t-test was used to calculate the statistical significance (***p < 0.001).

c, Imaging of phase transitioned complexes. Homer3 (H), Lphn3 (E31 and E32), PSD95 (P), and Shank3 (S) were labeled by NHS-ester fluorophore 405, 488, 546, 647, respectively, while GKAP (G) was unlabeled.

d, Quantification of the Lphn3 (top) and Shank3 fluorescence signal (bottom) across the phase-separated droplet illustrating the surface localization of Lphn3 E31 on the droplet filled with Shank3. Data are means ± SEM (n = 3 independent experiments).

e, Quantification of the sizes of phase-transitioned droplets formed by postsynaptic scaffold proteins GKAP/Homer3/PSD95/Shank3 (G/H/P/S) in the absence of Lphn3 or in the presence of Lphn3 E31 or Lphn3 E32.

f, Representative images of phase-transitioned postsynaptic scaffold protein complexes containing Lphn3 E31 that were clustered by presynaptic ligands Tenm2 and Flrt3.

g, Quantification of the clustering effect of presynaptic Tenm2 and Flrt3 ligands on Lphn3 E31 coated, phase-transitioned postsynaptic scaffolding protein complexes. Data are means ± SEM (n = 3 independent experiments).

h, Contribution of individual postsynaptic scaffold protein to phase transitions in the presence of Lphn3 containing Exon 31. Individual scaffold proteins were omitted during the phase separation and droplets were subjected to the same imaging condition as above.

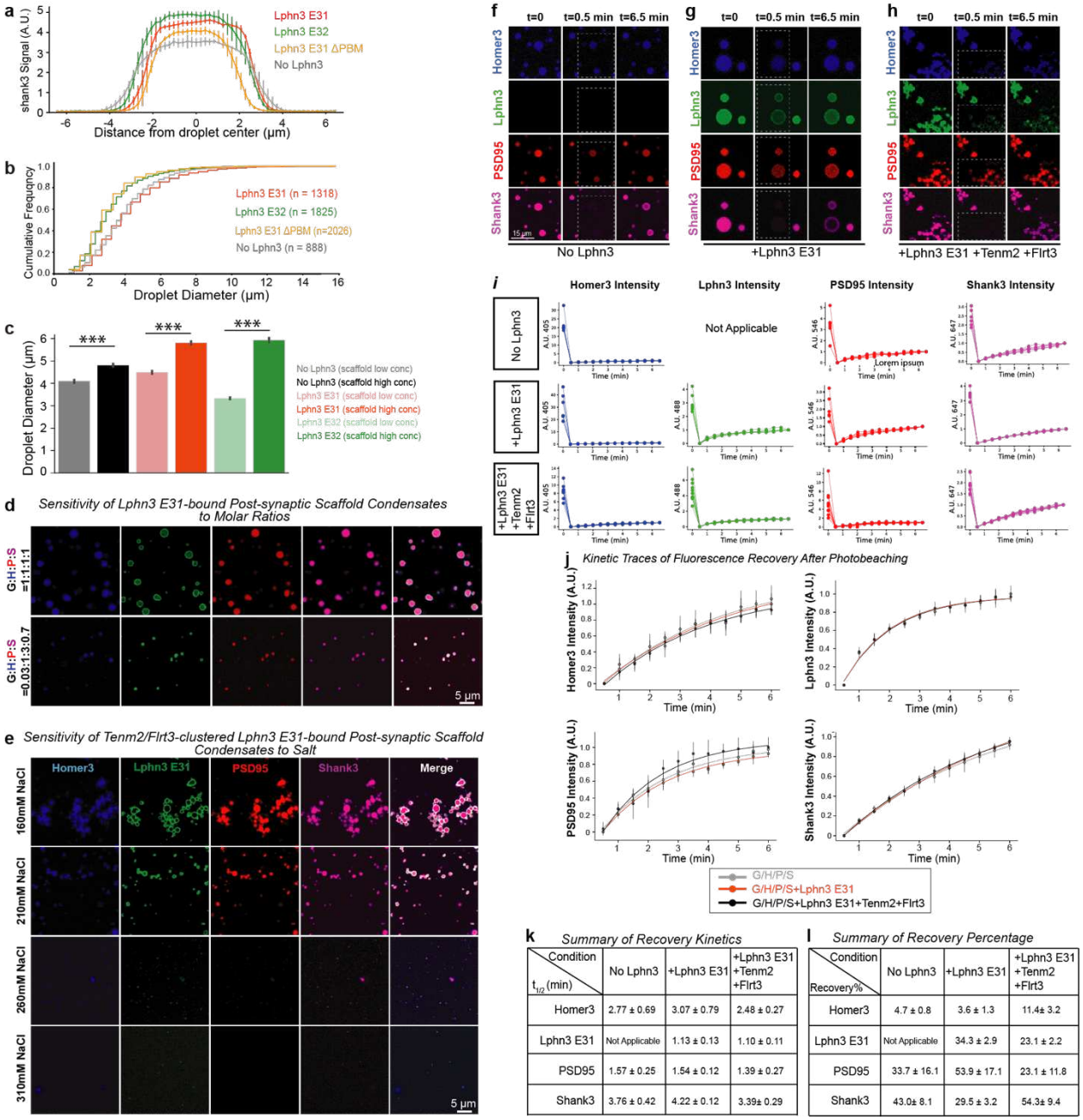

k *Summary of Recovery Kinetics*

Condition / $t_{1/2}$ (min)	No Lphn3	+Lphn3 E31	+Lphn3 E31 +Tenm2 +Flrt3
Homer3	2.77 ± 0.69	3.07 ± 0.79	2.48 ± 0.27
Lphn3 E31	Not Applicable	1.13 ± 0.13	1.10 ± 0.11
PSD95	1.57 ± 0.25	1.54 ± 0.12	1.39 ± 0.27
Shank3	3.76 ± 0.42	4.22 ± 0.12	3.39± 0.29

l *Summary of Recovery Percentage*

Condition / Recovery%	No Lphn3	+Lphn3 E31	+Lphn3 E31 +Tenm2 +Flrt3
Homer3	4.7 ± 0.8	3.6 ± 1.3	11.4± 3.2
Lphn3 E31	Not Applicable	34.3 ± 2.9	23.1 ± 2.2
PSD95	33.7 ± 16.1	53.9 ± 17.1	23.1 ± 11.8
Shank3	43.0± 8.1	29.5 ± 3.2	54.3± 9.4

<u>Extended Data Figure 8</u>: Further characterization of phase-separated, Lphn3-E31 coated post-synaptic scaffold condensates (a-d) and detailed FRAP (fluorescence recovery after photobleaching) experiments of phase-separated postsynaptic scaffolds without or with Lphn3 recruitment (e-k)

a, Quantification of the Shank3 fluorescence signal (bottom) across the phase-separated droplet illustrating the surface localization of Lphn3-E31 on the droplet filled with Shank3. Data are means ± SEM (n = 3 independent experiments). Also see Figure 4d, 4e.

b, Quantification of the sizes of phase-transitioned droplets formed by postsynaptic scaffold proteins GKAP/Homer3/PSD95/Shank3 (G/H/P/S) in the absence of Lphn3, or in the presence of Lphn3-E31, Lphn3-E32 or Lphn3-E31 ΔPBM.

c, Comparison of droplet sizes using different concentrations of scaffold proteins. Source data from ED Figure 7e and ED Figure 8b. A two-sided Student's t-test was used to calculate the statistical significance (***$p < 0.001$).

d, Sensitivity of phase separation to the stoichiometry of scaffold proteins. Physiological molar ratio[6] GKAP : Homer3 : PSD95 : Shank3 = 0.03125 : 1 : 3.09 : 0.73 was used.

e, Sensitivity of phase separation to ionic strength.

f-h, Representative images from Fluorescence Recovery After Photobleaching (FRAP) experiments at the indicated timepoints, with the target area (inset) bleached at 0.5 min.

i, Fluorescence intensity of all channels during the recording period of FRAP experiments for a given conditions. Each trace represents one independent experiment (n=6-10).

j, Recovery traces plotted as the mean ± SD (n=6-10) were fitted to exponential equation to extrapolate $t_{1/2.}$ Also see method.

k& **l**, Summary of recovery kinetics and percentage.

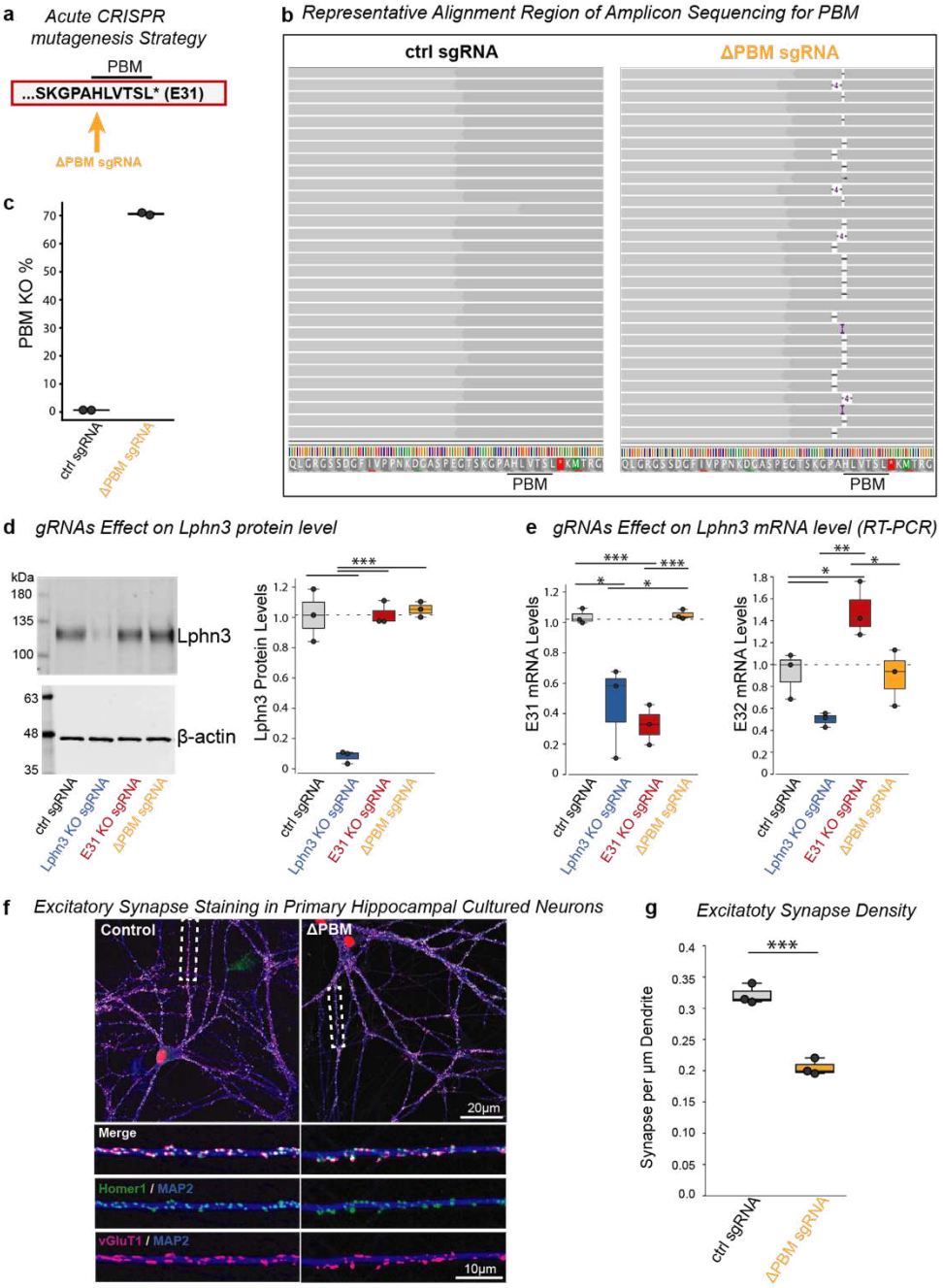

Extended Data Figure 9: Selective deletion of the PDZ-domain binding motif (PBM) in Exon31 of the Lphn3 gene decreases synapse numbers

a, Experimental strategy for the selective deletion of the PBM of Lphn3-E31. A gRNA targeting the genomic DNA that encodes the PBM in Exon31 was identified and used in acute CRISPR experiments in primary hippocampal cultures. (ΔPBM)

b, Monitoring the efficiency of CRISPR-mediated deletion of the PBM in cultured neurons. Total RNA from edited neurons was extracted, converted to cDNA. Then the PBM region was amplified for Miseq analysis. The interactive Genome Viewer (v2.16.2) image shows a representative alignment of sequences near the PBM region from neurons subjected to CRISPR with the control and the ΔPBM gRNA.

c, Quantification of PBM KO efficiency. Insertion/deletion which caused frameshift of the coding region, and mutation within the PBM region were classified as PBM KO events.

d, Lphn3 immunoblots showing that both the Exon-31-specific KO (E31 KO) or ΔPBM gRNA do not change Lphn3 protein levels, whereas the Lphn3 KO ablates Lphn3 expression. Each data point represents one independent culture (n=3); A two-sided Student's t-test was used to calculate the statistical significance (***$p < 0.001$).

e, RT-PCR demonstrates that the E31 KO and Lphn3 KO similarly ablate expression of Exon 31-containing Lphn3 mRNAs (left) but have opposite effects on Exon 32-containing Lphn3 mRNAs (right), whereas the PBM deletion (ΔPBM) does not change Exon31 or Exon32 mRNA levels. A two-sided Student's t-test was used to calculate the statistical significance (*$p < 0.05$; **$p < 0.01$; ***$p < 0.001$).

f & **g**, Selective deletion of the Lphn3 PBM significantly decreases the excitatory synapse density (**f**, representative images of cultured hippocampal neurons stained with antibodies to vGluT1, Homer1 and MAP2; **g**, summary graph of the density of puncta that were positive for both vGluT1 and Homer1). Each datapoint represents an independent culture (n=3); two-sided Student's t-test was used to calculate statistical significance (***$p < 0.001$).

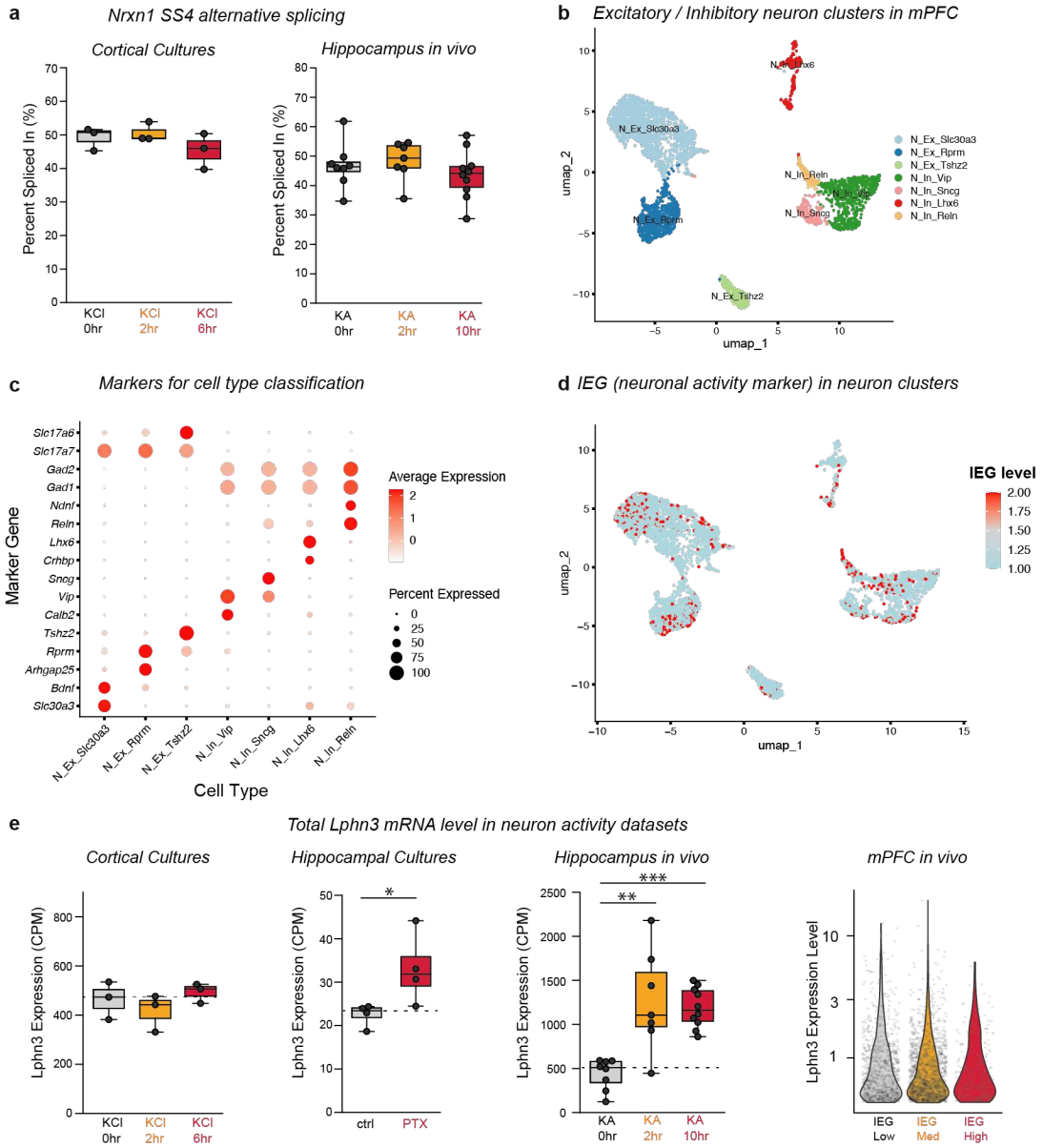

Extended Data Figure 10: Additional analyses of the activity-dependent splicing of Lphn3 Exon31 and Exon32

a, Neuronal activity does not change the Nrxn1 SS4 splicing level, as reported before[7]. This serves as a negative control to ensure that the strong activation conditions (KCl and kainate) used did not impair neuronal survival.

b, UMAP plot illustrating the clustering of neurons (NeuN$^+$) into subtypes of excitatory and inhibitory groups in a single-cell RNAseq dataset obtained from the mPFC[4]. N, neuron; Ex, excitatory; In, inhibitory. Scl30a3, Rprm, Tshz2 are markers identifying distinct groups of excitatory neurons, while Vip, Lhx6 and Reln are markers identifying distinct groups of inhibitory neurons.

c, Expression levels of the indicated marker genes in different types of excitatory and inhibitory neurons in the mPFC single-cell RNaseq dataset.

d, Mapping of the expression levels of immediate early genes (IEG) as activation markers onto the neuron types identified in the UMAP plot of b.

e, Total Lphn3 levels determined in the various RNAseq datasets used for the analysis of activity-dependent alternative splicing of Lphn3. Wilcoxon rank-sum test was used to calculate statistical significance (*$p < 0.05$; **$p < 0.01$; ***$p < 0.001$).

References

1. Ray, T. A. *et al.* Comprehensive identification of mRNA isoforms reveals the diversity of neural cell-surface molecules with roles in retinal development and disease. *Nat. Commun.* **11**, 1–20 (2020).

2. Furlanis, E., Traunmüller, L., Fucile, G. & Scheiffele, P. Landscape of ribosome-engaged transcript isoforms reveals extensive neuronal-cell-class-specific alternative splicing programs. *Nat. Neurosci.* **22**, 1709–1717 (2019).

3. Tasic, B. *et al.* Shared and distinct transcriptomic cell types across neocortical areas. *Nature* **563**, 72–78 (2018).

4. Sun, W. *et al.* Spatial and single-cell transcriptomics reveal neuron-astrocyte interplay in long-term memory. *bioRxiv* 1–51 (2023) doi:10.1101/2023.03.20.533566.

5. Araç, D. *et al.* A novel evolutionarily conserved domain of cell-adhesion GPCRs mediates autoproteolysis. *EMBO J.* **31**, 1364–1378 (2012).

6. Helm, M. S. *et al. A large-scale nanoscopy and biochemistry analysis of postsynaptic dendritic spines*. *Nature Neuroscience* vol. 24 (Springer US, 2021).

7. Liakath-Ali, K. & Südhof, T. C. The Perils of Navigating Activity-Dependent Alternative Splicing of Neurexins. *Front. Mol. Neurosci.* **14**, 1–19 (2021).